Measurement report: New Particle Formation Events Observed during the COALA-2020 Campaign

Jhonathan Ramirez-Gamboa[1,2], Clare Paton-Walsh[1*], Melita Keywood[2], Ruhi Humphries[2], Asher Mouat[4], Jennifer Kaiser[4,5], Malcom Possell[3], Jack Simmons[1], Travis A. Naylor[1]

[1] Centre for Atmospheric Chemistry, School of Earth, Atmospheric and Life Sciences, University of Wollongong, NSW 2522, Australia

[2] Climate Science Centre, CSIRO Environment, Aspendale, VIC 3195, Australia

[3] School of Life and Environmental Sciences, University of Sydney, NSW 2006, Australia

[4] School of Civil and Environmental Engineering, Georgia Institute of Technology, Atlanta GA 30332, USA

[5] School of Earth and Atmospheric Sciences, Georgia Institute of Technology, Atlanta GA 30332, USA

* Correspondence: clarem@uow.edu.au

Abstract:

Aerosols play an important role in atmospheric processes influencing cloud formation, scattering and absorbing solar radiation, and ~~play an important role~~ in chemical reactions affecting the abundance of trace gases in the atmosphere. Ultimately aerosols affect the radiative balance of the earth modifying climate. A large fraction of aerosols is formed through chemical reactions following gas-to-particulate processes in the atmosphere: nucleation~~, condensation~~ and growth. Biogenic Secondary Organic Aerosols (BSOA) are formed when plant produced volatile organic compounds (VOCs) react in the atmosphere through gas-phase oxidation~~ heterogeneous reactions~~. One of the highest BVOC emitting regions in the world is South-east Australia due to the high density of *Eucalyptus* species. The COALA-2020 (Characterizing Organics and Aerosol Loading over Australia) campaign worked towards a better understanding of biogenic VOCs in quasi-pristine conditions in the atmosphere and their role in particle formation.

The observations showed a highly reactive atmosphere with frequent new particle formation (NPF) occurring (42~~50~~% days with data) often associated with pollution plumes. Analysis of NPF events suggested that SO_2 plumes likely triggered particle formation, while particle growth depended on available VOCs, hydroxyl radicals ~~(influenced by relative humidity),~~ and the presence of multiple SO_2 intrusions promoted growth of smaller clusters. Nighttime NPF events coincided with monoterpene ozonolysis~~. One nighttime NPF event showed potential isoprene nitrate oxidation enhancing growth, but the limited night-time data hindered conclusive interpretations.~~ but where rare. These findings highlight the significant role of biogenic VOCs, in driving NPF and SOA formation in South-east Australia~~, even after major wildfires~~. The COALA-2020 campaign provided valuable insights into local atmospheric chemistry and its potential impact on regional air quality and climate. However, longer-term observations are crucial to understand seasonal variations, trends and extreme events.

Keywords: COALA-2020; aerosols, BVOCs, NPF.

1. Introduction

Aerosols can influence our health (Annesi-Maesano et al., 2013; Shi et al., 2016) but also play an important role in regulating Earth's energy balance, the hydrological cycle and even the abundance of key chemical

species in the atmosphere such as hydroxyl radical (OH) and indirectly greenhouse gases (e.g., Kerminen et al., 2012). The chemical composition, size and concentrations of aerosols determine the effects on health and the environment (Liu et al., 2016b; Pope and Dockery, 2006; Ren et al., 2017). Aerosols can be directly emitted (primary aerosols) or they can be product of chemical reactions in the atmosphere (secondary aerosols) (Pöschl, 2005).

Secondary aerosols are produced via gas-to-particle transition. New Particle Formation (NPF) occurs when multiple reactions in the atmosphere create stable molecular clusters. Once the clusters are formed, they can grow through coagulation and condensation potentially resulting in cloud condensation nuclei (CCN) (Dal Maso et al., 2005; Hussein et al., 2005; Kulmala et al., 2001). Multiple factors determinate NPF in the atmosphere including atmosphere composition and boundary conditions (temperature, humidity, planetary boundary layer (PBL) height, turbulence) (Bousiotis et al., 2021; Wu et al., 2021; Xu et al., 2021a). Sulfuric acid (H_2SO_4) is one of the main drivers of the nucleation process in the continental boundary layer, but it does not explain all growth and nucleation rates (Sihto et al., 2006). The presence of ammonia (NH_3), amines or ions in the atmosphere can enhance H_2SO_4 nucleation rates (Kirkby et al., 2023; Zhao et al., 2011; Zheng et al., 2015). High levels of SO_2 and Volatile Organic Compounds (VOCs) ~~in a humid atmosphere~~ will enhance NPF (Nestorowicz et al., 2018; Song et al., 2019, p.20; Xu et al., 2021b).

VOCs are a group of carbon-based gases emitted by biological and anthropogenic sources that are characterised by their high vapour pressure (Goldstein and Galbally, 2007; Kesselmeier and Staudt, 1999; Matsui, 2006). VOCs can undergo hydroxyl radical (OH), ozone or nitrate radical (NO3) oxidation in the gas phase, producing compounds of varying volatilities, and products with low enough volatility can contribute to NPF or partition to existing particles, resulting in particle growth.

~~-~~The most common biogenic VOC (BVOC) is isoprene followed by monoterpenes. BVOCs play an important role in secondary organic aerosol (SOA) formation (e.g., Mahilang et al., 2021). VOCs have been associated with particle growth (Riipinen et al., 2012) but their role and the autoxidation mechanism was not understood until recently (Bianchi et al., 2019). Autoxidation of monoterpenes supports the particle growth process by generating highly oxygenated molecules (HOMs) via the formation of peroxy radicals (Bianchi et al., 2019; Kirkby et al., 2023; Lehtipalo et al., 2018~~, p.201~~). HOMs can be characterised as ultra-low VOCs (ULVOC) or extremely low VOCs (ELVOC) depending upon the saturation concentration ~~at 298K.~~(Bianchi et al., 2019; Peräkylä et al., 2020).

~~While~~ Oxidation of monoterpenes is a significant pathway for ~~oxidation of monoterpenes produces higher~~ SOA formation, yielding higher amounts of low-volatility molecules like ULVOCs and ELVOCs compared to isoprene oxidation ~~formation yields than isoprene resulting to the formation of ULVOC or ELVOC molecules during OH or ozonolysis oxidation~~(Friedman and Farmer, 2018; Lee et al., 2023; Luo et al., 2024; Riva et al., 2019; Zhang et al., 2018)~~.~~ HOMs are key precursors for new particle formation. However, the atmospheric production of HOMs can be limited by competing reactions and the presence of other VOCs. For instance, as a general principle, once a VOC molecule oxidizes, it becomes more complex and forms larger Oxygenated VOCs (OVOCs) that are less likely to undergo further oxidation, especially in the presence of other VOCs with higher reactivity towards OH or O_3 (Kiendler-Scharr et al., 2009). An example of this limitation is the suppression of monoterpene-derived HOM formation by isoprene oxidation products. These products can interfere with the formation of C_{20} dimers from monoterpene oxidation, leading to a reduced yield of HOMs

Field Code Changed
Formatted: Spanish (Spain)
Field Code Changed
Field Code Changed
Formatted: English (Australia)
Formatted: English (Australia)
Formatted: Subscript

and favoring the formation of weaker nucleating species C_{15} (Dada et al., 2023; Heinritzi et al., 2020; Liu et al., 2016a). This suppression effect is dynamic, varying non-linearly with local atmospheric composition (e.g., isoprene and monoterpene concentrations, oxidant availability) and atmospheric conditions (e.g., temperature, humidity, stability), which ultimately determine the dominant SOA formation pathways (e.g. Song et al., 2019). ~~under the right conditions, isoprene can also lead to SOA formation (e.g. Fry et al., 2018). Isoprene oxidation products can oxidise to LVOC promoting particle growth in the larger sizes (above 3 nm) (Heinritzi et al., 2020). For example, the SOA yield of isoprene oxidised with the nitrate radical at night generates several times the yield observed through the OH oxidation path (e.g. Ng et al., 2008). Recent studies suggest that in biogenic-rich regions isoprene SOA yield in low NO_x environments can be much higher than previously reported when considering further oxidation of the products (e.g. Liu et al., 2016a), promoting the formation of extremely low or low volatility organic compounds (ELVOC and LVOC respectively) important for particle grow.~~

~~Isoprene, monoterpenes, OH and nitrate radical and ozone availability in the atmosphere are key to promoting SOA formation (e.g. Song et al., 2019). As a VOC molecule oxidises it becomes more complex and a larger oxygenated VOC (OVOC),so is less likely to be oxidised again, particularly when in the presence of other VOCs with higher OH reactivity (Kiendler-Scharr et al., 2009). HOMs are key for nucleation, but HOM production in the atmosphere is limited by other reactions/byproducts. Isoprene NPF suppression is one of those cases in which isoprene oxidation products limit the formation of C_{20} dimers and reduce the yield of highly oxygenated molecules (HOMs) in favour of weaker nucleators C_{15} (Dada et al., 2023; Heinritzi et al., 2020; Liu et al., 2016a). This effect is non-linear nor constant and will change with local conditions.~~

Understanding BVOC emissions and their role in SOA formation is important to accurately predict aerosol properties and their impact on climate. However, BVOC are poorly characterized under Australian conditions (Paton-Walsh et al., 2022). MEGAN (The Model of Emissions of Gases and Aerosols from Nature) emissions show south-east Australia as one of the BVOC hot-spots in the region (Guenther et al., 2012) but multiple modelling studies have shown that MEGAN emissions estimation might not represent local conditions correctly in this region (Emmerson et al., 2016, 2018, 2019). Most of the Australian forested regions are dominated by high emitting *Eucalyptus* species (ABARES, 2019; Aydin et al., 2014; Padhy and Varshney, 2005) that combined with periods of high temperature and drought stress create the conditions for high emissions/concentrations of BVOCs in the atmosphere (Emmerson et al., 2020; Fini et al., 2017; Ormeño et al., 2007). The emissions ratios of isoprene to other VOCs are poorly constrained and the local chemistry is not well understood.

The COALA-2020 campaign worked towards a better understanding of biogenic VOCs in quasi-pristine conditions in the atmosphere and their role in local atmospheric chemistry in south-east Australia. COALA-2020 was a collaborative effort between local institutions including the University of Wollongong, CSIRO, ANSTO, and the University of Sydney, and international peers from Georgia Institute of Technology, The University of California, Irvine, Nagoya University and Lancaster University. This part of the study focused on identifying and characterising NPF events after the "Black Summer" 2019-2020 Australian bushfire season. Here we focus on identifying drivers and conditions in which NPF started or were enhanced in the local environment.

Formatted: Spanish (Spain)

Field Code Changed

Formatted: First Paragraph

2. Materials and Methods

2.1 The COALA-2020 Campaign

The COALA-2020 campaign took place at Cataract Scout camp (34°14'44" S, 150°49'26" E) located 20 km north-northwest of Wollongong on the east coast of NSW, Australia. The site is surrounded by a heavily forested area mainly stocked by Eucalyptus species (see Figure 1~~Figure 1~~~~Figure 1~~). North of the sampling site is a four-lane arterial road connecting the M1 motorway on the east coast with south-western Sydney. Other possible anthropogenic sources impacting the site are two underground coal mine heads, located 1.5 km to the northeast and 2.5 km to the north). Further afield sources include the Sydney suburban area (around 18 km north-west), Sydney city (45 km north), Wollongong urban area and Port Kembla steelworks in the southern part of Wollongong (28 km to the southeast).

The campaign was conducted from the 17th January to the 23rd March, 2020. The first period of the campaign (17th January to 5th February) was heavily impacted by smoke pollution from the bushfires affecting the region. On 5th February, ~~A~~a substantial rain event extinguished the fires and cleared the atmosphere of residual smoke pollution (Mouat et al., 2022; Simmons et al., 2022). The smoke pollution period has been removed from the analysis presented here as we focus on understanding atmospheric processes during more normal conditions. Thus, this paper presents the analysis of BVOCs alongside anthropogenic emissions

Formatted: Font: (Default) +Body (Calibri), 12 pt, Not Italic, Font color: Auto

Formatted: Superscript

Formatted: Superscript

Formatted: Superscript

Formatted: Superscript

Formatted: Superscript

and their role in NPF during *the second part of the COALA-2020 ambient measurements campaign running from ~~5~~ February 5th until March 17th 2020.*

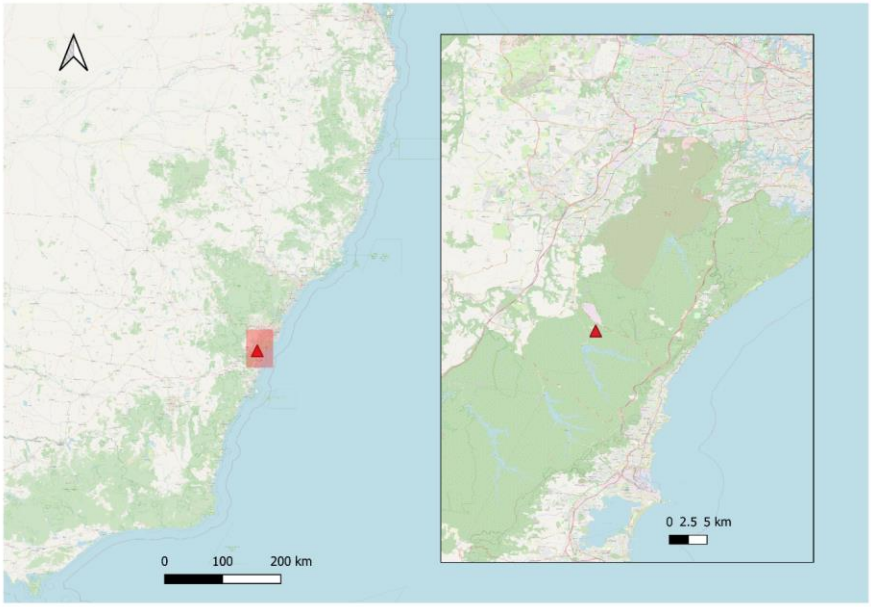

Figure 1 Location of the sampling site, to Sydney, NSW in the north. The sampling site had four different climate control containers for the instruments, as well as a soil sampling site around 50 meters northeast from the main sampling site and the High-Vol PM filter. "Map data copyrighted OpenStreetMap contributors and available from https://www.openstreetmap.org"

2.2 Instrumentation

The instruments deployed in the campaign are presented in Table 1~~Table 1~~Table 1. They included an air quality monitoring station owned and operated by the NSW Government Department of Climate Change, Energy, the Environment and Water (DCCEEW), located approximately 10 m away from the main sampling line for VOCs. This station included measurements of temperature, windspeed and direction, PM_{10}, $PM_{2.5}$, O_3, SO_2, NO_x, CO and visibility. Inlet heights on this station were between 4.5m to 5.6 m above ground level. All NSW air quality monitoring stations are accredited by the National Association of Testing Authorities (Australia), however it should be noted that these instruments are targeted at regulatory standards and are not research grade. In particular this means that measurements made close to the detection limits are likely to be inaccurate and should be interpreted as indicative measures rather than accurate quantitative measures of atmospheric concentrations.

VOCs were measured using a Proton Transfer Reaction Mass Spectrometer (Ionicon PTR-ToF-MS 4000) which operated with a mass range spanning m/z = 18-256. The drift tube was held at a temperature of 70° C, pressure at 2.60 mbar, and an electric field to molecular number density ratio of 120 Td. The instrument was housed in a separate climate-controlled unit. Samples were drawn from an inlet on a 10 m mast through a 20 m long PTFE line using a bypass flow of 1.2-3 L min^{-1}. Calibrations were made on site using standardized

Formatted: Font: (Default) +Body (Calibri), 12 pt, Not Bold

cylinders containing 17 compounds including isoprene, monoterpenes, methyl vinyl ketone (MVK) & methacrolein (MACR), benzene, C_8-aromatics, and C_9-benzenes (Mouat et al., 2022). Mass spectra were integrated to produce data at 1 minute temporal resolution. Mole fractions were further averaged on a five-minute basis.

A suite of aerosol instruments were operated within in the Atmospheric Integrated Research Facility for Boundaries and Oxidative eXperiment (AIRBOX) container (Chen et al., 2019). Sample air was drawn from a common aerosol bypass inlet. The inlet was located 5 m above ground level for the following instruments:

1. A Ultrafine Condensation Particle Counter (UCPC TSI 3776) was used to measure condensation nuclei number concentration greater than 3 nm (CN_3) (TSI Incorporated, Shoreview, MI, USA). The instrument was operated at a sample flow rate of 300 mL min^{-1}. Measurements were recorded at 1 Hz temporal resolution.

2. A Scanning Mobility Particle Sizer (SMPS) was used to measure aerosol size distribution between 14 and 670 nm mobility diameter. Full scans of this size range were recorded every five minutes. The system consisted of an X-ray aerosol neutralizer and 3071 Long Electrostatic Classifier (TSI Incorporated, Shoreview, MI, USA) coupled to a 3772 CPC (TSI Incorporated, Shoreview, MI, USA). Sample was drawn from the same inlet as used by the UCPC.

3. Chemical composition of aerosols with diameter smaller than 1 µm (PM_1) were taken using a Time-of-Flight Aerosol Chemical Speciation Monitor (ACSM; Aerodyne Research Inc., Billerica, MA, USA). Mass concentrations of organics (Org), sulphate (SO_4^{2-}), nitrate (NO_3^-), ammonium (NH_4^+), and chloride (Cl^-) in the aerosol fraction 40-1000 nm vacuum aerodynamic diameter range, referred to as PM_1, are reported. Measurements were taken at 10-minute resolution. Sample air was drawn from the aerosol inlet common to the CPC and SMPS and dried using a Nafion dryer to < 40% relative humidity before sampling.

Table 1: Instruments deployed during the COALA 2020 campaign and included in the present analysis.

Name of parameter	Instrument type
NO - NO_2 -NO_x	API T204
O_3	Ecotech 9810
PM_{10}	Thermo (TEOM) 1405A
$PM_{2.5}$	Thermo (BAM)5014i
SO_2	API T100
Black Carbon	Magee Scientific Aethalometer AE33
VOCs	PTR-ToF-MS (Ionicon)
CO - CO_2 - CH_4 - N_2O	FTIR in situ analyser
CN_3	TSI 3776
Particle number size distribution (14 nm to 660 nm)	SMPS
PM_1 mass composition	Tof-ACSM, Aerodyne
Wind Speed and Wind Direction	2D Ultrasonic anemometer
Temperature, Relative humidity	Vaisala HMP155
Photosynthetic active radiation (PAR)	

2.3 NPF Classification Method

The method proposed by Dal Maso et al. (2005) was used to classify the particle size distribution data. To apply the method the particle number density plots were made for each day during the campaign and the plots were visually inspected to identify if an event occurred on that day. A day of data was classified as an *event* if there was nucleation, and growth up to 25nm for at least two hours.

Once the events were classified, a logarithmic fit was applied to determine the geometric diameter of each mode. The data was manually divided in chunks of 10 minutes to visually inspect and determine the number of modes and the geometrical diameter range of each event (nucleation <25 nm, Aitken 25 nm -100 nm, accumulation >100 nm). Once those parameters were defined and included in the code, each event was divided in periods of time with similar distribution modes.

For illustration a hypothetical event lasting two hours was divided in two: one hour with simultaneous two particle modes (nucleation and Aitken) and then one hour with just one particle mode (Aitken). This is done to estimate an accurate geometrical particle diameter based on the number of modes. This avoided the problems of changes in the number of modes in the sample. Finally, the data was merged again to have a time series of number of particles predicted with the fit, number of modes predicted and geometrical particle diameter.

The algorithm works by providing the number of modes observed in the input dataset. Then it selects the provided model equation for each mode number and iterates over a hundred fits looking for the best fit. The Bayesian Information Criterion (BIC) was used to identify the best fit, looking for the lowest values. Once the best fit was selected, the total particle number estimated by the model was compared with the sample record for each sample to assure it was within a 5 % difference compared to the total particle number reported in the sample. The result was then visually checked looking for the geometrical diameter and how it compares to the distribution size plots from the raw aerosol distribution size data. Once the model was considered representative and accurate enough, the growth rate for each event was determined using a simple linear regression of the change in the geometrical diameter in time from nucleation to Aitken and eventually to accumulation mode.

3. Results and Discussion

3.1 Frequency of NPF Events

Of the 40 days included in the analysis, nine days didn't have any data. Of the 31 days with data, 12~~4~~ (39~~45~~%) showed clear NPF events, nine~~nine~~ (29%) were considered undefined and ten~~, eight~~ (32~~26~~%) didn't have enough data or were classified as a non-event The percentage of days with NPF is similar to those of other sites in forested areas in the Northern Hemisphere (Kalkavouras et al., 2020; Uusitalo et al., 2021). 39~~45~~% of days with NPF events and 29% with undefined events implies a highly reactive atmosphere even in this rural area with some anthropogenic influence of mobile sources and occasionally coal-fired power plant in the Hunter Valley region.

~~An example of the time series of an NPF event is shown in~~ Figure 2 ~~Figure 2~~ illustrates the time series of an NPF event observed on 11th February 2020. The NPF event commenced at 8 am, preceded by a peak in both SO_2 concentrations and the estimated H_2SO_4 proxy.~~for the event on 11 Feb 2020. The NPF commences at 8~~

Formatted: Font: (Default) +Body (Calibri), 12 pt, Font color: Auto, English (United States)

Formatted: Superscript

Formatted: Subscript

Formatted: Subscript

Formatted: Subscript

~~am shortly before which a peak is observed in SO_2 and the H_2SO_4 proxy~~ The shaded area in the plot highlights the growth period which is marked by an increase in mode diameter and condensation sink. Ozone is also increasing at this time. The increase in aerosol SO_4^{2-} and organics during this period shows the influence of this reaction chemistry on particles larger than 100 nm in the aerosol size distribution. We estimated the H_2SO_4 proxy using the rural model developed by ~~(~~Dada et al.~~,~~ (2020). This model was chosen from among the options because the environmental conditions under which it was derived are the most similar to those of our sampling site. The equation used to estimate H_2SO_4 proxy was

$$[H_2SO_4]_{\{rural\}} = -\frac{CS}{2*(2x10^{-9})} + \left[\left(\frac{CS}{2*(2x10^{-9})}\right)^2 + \frac{[SO_2]}{(2x10^{-9})} * (9 * 10^{-9} * GlobRad]^{\frac{1}{2}}\right.$$

Where CS is the condensation sink, SO_2 is the concentration of SO_2, GlobRad is the global radiation obtained from the Photosynthetic Photon Flux Density (PPFD) values as GlobRad = 0.327*PPFD.

~~(estimated using the rural proxy proposed by Dada et al. 2020). The shaded area in the plot highlights the growth period which is marked by an increase in mode diameter and condensation sink. Ozone also increases in this time. The increase in aerosol SO_4 and organics during this period shows the influence of this reaction chemistry on particles larger than 100 nm in the aerosol size distribution~~

~~**3.2 Triggers for NPF Events**~~

~~Of the fourteen days with NPF, five occurred during the night or early morning (before sunrise), and nine during the day. The time series of SO_2, NO_x, ozone, VOCs and the aerosol composition were used to identify which variables triggered and influenced the aerosol formation and growth. Of the fourteen event days of NPF, eight days include VOC data and nine days include aerosol composition data, noting that the composition data is not applicable to particles <100 nm and only three events led to accumulation sized particles (diameter >100 nm).~~

~~From the daily time series of all available variables over the 14 days of NPF events, it is evident that SO_2 frequently triggers or at least influences the particle formation. However, the trigger for nighttime events is less clear. To group the common factors influencing NPFs for daytime and night-time events, a comparison of the growth rate was used to determine whether the rates were similar during the day and during the night.~~

Formatted: Subscript
Formatted: Subscript
Formatted: Font: Not Bold
Formatted: Subscript
Formatted: Subscript
Formatted: Subscript
Formatted: Subscript

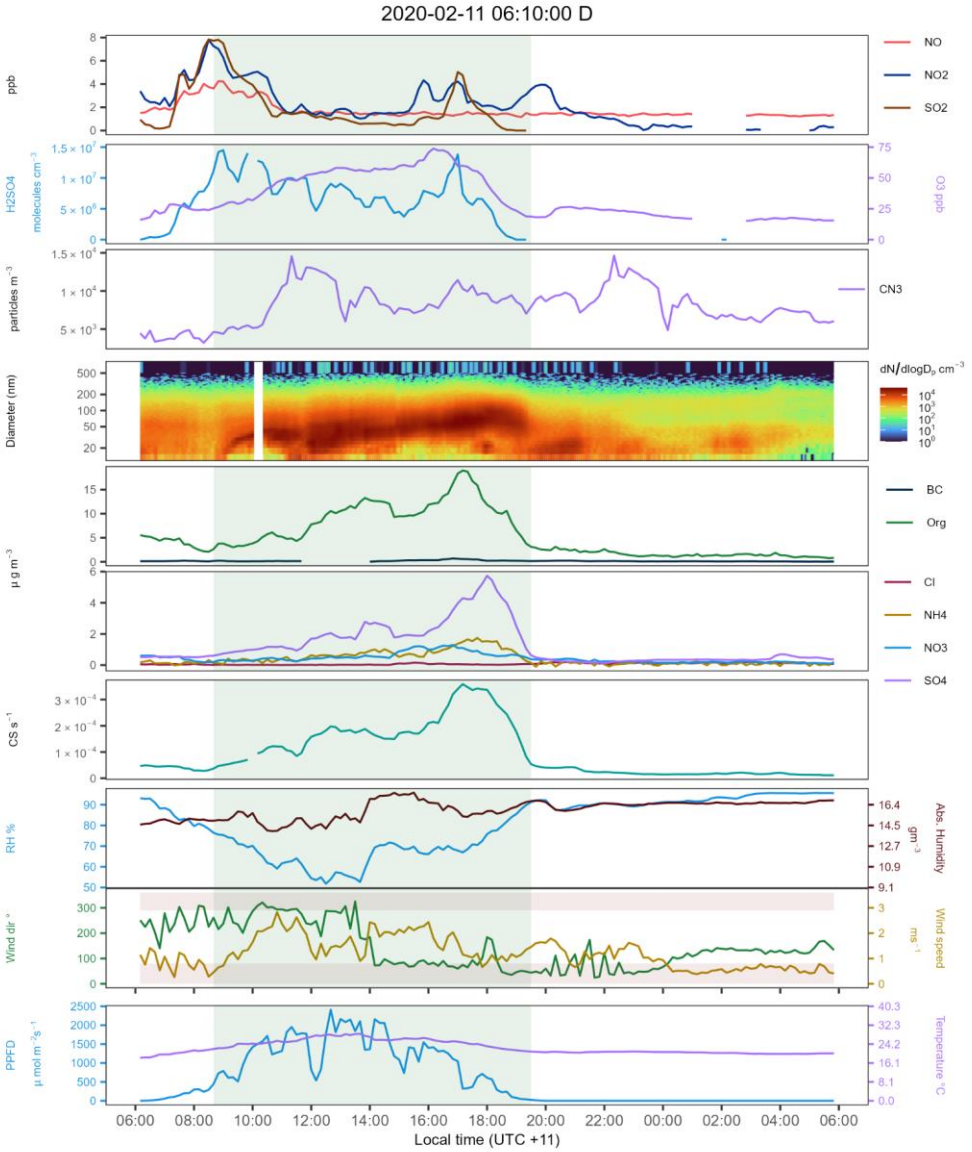

Figure 2 Time series for all selected variables during the NPF event during 2020-02-11. NO = Nitric oxide, NO_2 = Nitrogen dioxide, SO_2 = Sulphur dioxide, H_2SO_4 = Sulphuric acid, O_3 = Ozone, CN_3 = Condensation Nuclei >3nm, CN_3-CN_{14} = difference of CN_3 minus the sum of all channels from the SMPS data. BC = Black carbon. Org = Organic mass fraction, NH_4 = Ammonium mass fraction, NO_3 = Nitrates mass fraction,

250

251

252

253

254

Formatted: Subscript

Formatted: Subscript

Formatted: Subscript

Formatted: Subscript

Formatted: Subscript

Formatted: Subscript

Formatted: Subscript

Formatted: Subscript

Formatted: Subscript

Formatted: Subscript

Formatted: Subscript

SO_4^{2-} = Sulphates mass fraction, Cl = Chloride mass fraction. CS = condensation sink. PFFD = Photosynthetic Photon Flux Density. VOCs mole fractions were not available during this specific event. Note how the fraction of organics, sulphates and ammonium increase with a positive correlation, dominating over the nitrate and chloride fractions until the end of the event. The light green area marks the NPF, and growth period mentioned in the analysis. the brown shade areas in the wind panel highlight areas where the wind comes from the nearby roads. Note that the NO values are close to detection limit and look biased high and hence should be interpreted as an indicative rather than accurate quantitative measure of atmospheric concentration.

3.2 Triggers for NPF Events

Of the ~~fourteen~~twelve days with NPF, four~~ive~~ occurred during the night or early morning (before sunrise), and eight~~nine~~ during the day. The time series of SO_2, NO_x, ozone, VOCs and the aerosol composition were used to identify which variables triggered and influenced the aerosol formation and growth. Of the ~~fourteen~~twelve event days of NPF, ~~eight~~six days include VOC data and ~~nine~~eight days include aerosol composition data, noting that the composition data is not applicable to particles <100 nm and only three events led to accumulation sized particles (diameter >100 nm). The data available for each event is summarised in *Table* 2~~Table 2~~.

Table 2~~2~~ Data available for each NPF event identified during the COALA campaign

Event	time	NOx	O_3	SO_2	VOCs	CN_3	SMPS	ACSM
05/02/2020	N	✓	✓	✓	✓	✓	✓	
10/02/2020	N	✓	✓	✓		✓	✓	✓
11/02/2020	D	✓	✓	✓		✓	✓	✓
15/02/2020	D	✓	✓	✓		✓	✓	✓
16/02/2020	D	✓	✓	✓		✓	✓	✓
24/02/2020	N	✓	✓	✓		✓	✓	✓
06/03/2020	D	✓	✓	✓	✓	✓	✓	✓
07/03/2020	D	✓	✓	✓	✓	✓	✓	✓
08/03/2020	D	✓	✓	✓	✓		✓	✓
09/03/2020	N	✓	✓	✓		✓	✓	
10/03/2020	D	✓	✓	✓	✓	✓	✓	
11/03/2020	D	✓	✓	✓	✓		✓	

From the daily time series of all available variables over the 12~~4~~ days of NPF events, it is evident that SO_2 frequently triggers or at least influences the particle formation. However, the trigger for nighttime events is pointing to NO_2 related chemistry but without complementing measurements it's unclear~~less clear~~. To group the common factors influencing NPFs for daytime and night-time events, a comparison of the growth rate was used to determine whether the rates were similar during the day and during the night.

Formatted: Subscript
Formatted: Superscript
Formatted: Font: 9 pt, Font color: Auto, English (Australia)
Formatted: Font color: Auto, English (Australia)
Formatted: Caption, Centered, Keep with next
Formatted: Subscript
Formatted: Subscript
Formatted: Subscript
Formatted Table
Formatted: Body Text, Left
Formatted: Subscript
Formatted: Body Text

3.3 Particle Growth Rates during daytime and nighttime events

The estimated growth rate is presented in Figure 3~~Figure 3~~Figure 3. Only four of the nine events during daytime (upper panel of Figure 3~~Figure 3~~Figure 3) had a representative Pearson coefficient (R>0.6), the remaining five events did not have a stable linear growth and are not shown in the plot. The events which showed unstable growth patterns suggests a highly variable condensation source, possibly resulting from changing H_2SO_4 concentrations. This is complicated further by changing wind directions.

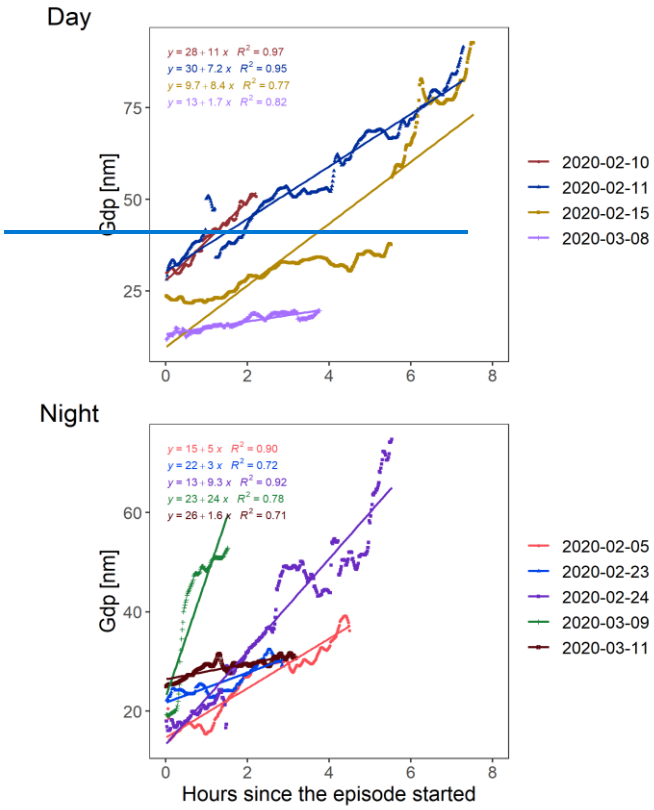
Day
y = 28 + 11 x R² = 0.97
y = 30 + 7.2 x R² = 0.95
y = 9.7 + 8.4 x R² = 0.77
y = 13 + 1.7 x R² = 0.82
Gdp [nm]
75
50
25
0
2
4
6
8
2020-02-10
2020-02-11
2020-02-15
2020-03-08
Night
y = 15 + 5 x R² = 0.90
y = 22 + 3 x R² = 0.72
y = 13 + 9.3 x R² = 0.92
y = 23 + 24 x R² = 0.78
y = 26 + 1.6 x R² = 0.71
Gdp [nm]
60
40
20
0
2
4
6
8
Hours since the episode started
2020-02-05
2020-02-23
2020-02-24
2020-03-09
2020-03-11

285

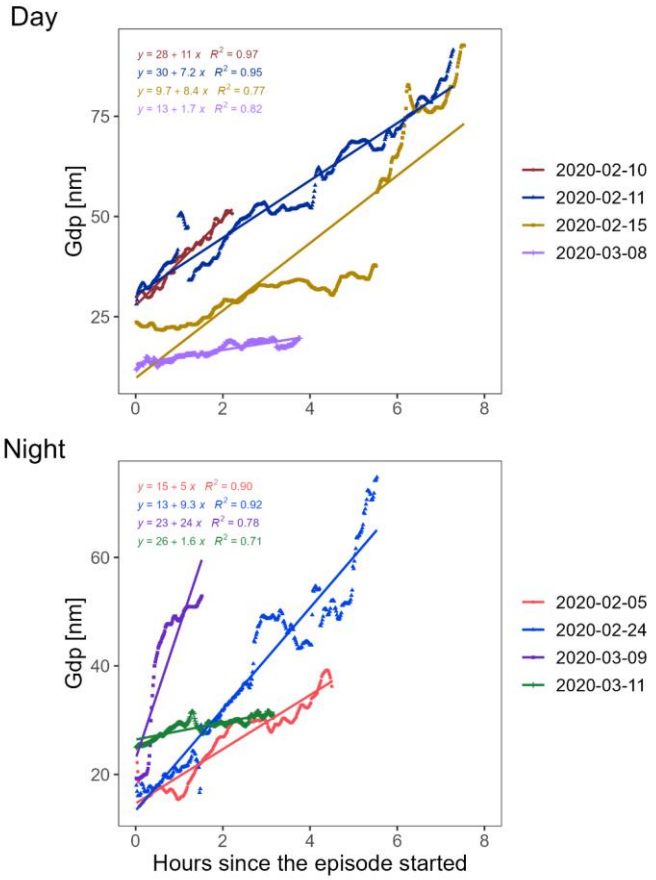

Figure 3: Geometric particle diameter evolution in each event where the logarithmic fit converged. The top panel presents the daytime data (only four events converged to a statistically significant model). The bottom panel presents the nighttime events.

Some events highlight how the dynamic nature of daytime concentrations of O_2, NO_2 and O_3 complicate the analysis (see figure S1). Nonetheless, these events provide insight into the factors that may drive the growth and particle formation and so were included in all the analysis. Event 2020-02-15 in Figure 3~~Figure 3~~ is an example of how the geometric particle diameter can change when there is rapid growth. The first part of the regression shows slower growth rate. After the 6th hour of slow growth, the rate increases substantially, attributed to an increase of H_2SO_4 around this time. Shortly after this accelerated growth, there is a wind change from northerly to southerly (Figure S4). Following the southerly wind shift, a lower condensation sink and higher relative humidity likely contributed to the Gdp increase via enhanced condensation and water

Formatted: Font: (Default) +Body (Calibri), 12 pt, Font color: Auto

Formatted: Subscript

Formatted: Subscript

uptake. Declining tracer levels ~~(of what)?~~SO_2 and NO_x indicate that local particle growth mechanisms were likely dominant over the influence of a new air mass up to the 7th hour when increases in NO_x and SO_2 are observed. ~~.~~

In contrast to the daytime events, all the night-time events were stable enough to determine the event growth rate. The growth rate varied considerably between events (see lower panel of Figure 3~~Figure 3~~) and most likely reflects differences in the factors driving the particle formation between these episodes. The specific oxidation pathways that were active during each event likely had a direct impact on the observed differences in growth rates. These ~~The differences in the growth rate might be directly affected by the main oxidation pathways available at the time of the reaction. These~~ reaction pathways might include ~~isoprene oxidation by nitrate radical (NO_3) oxidation path during the night (Wu et al., 2021b),~~ monoterpene ozonolysis and condensation over previously formed clusters (Liu et al., 2023; Wang et al., 2023), or oxygenated VOCs (OVOCs) brought to the site and condensed on formed seeds or ~~starting~~may initiate nucleation (Bianchi et al., 2019; Higgins et al., 2022). Some of these processes were observed during the campaign and will be further explored on the nighttime events section.

3.4 Daytime NPF Events

From the timeseries analysis of all daytime events (see Figure 2~~Figure 2~~~~Figure 2~~, 5-6~~8~~ and supplementary figures S1-S4~~5~~), four key points were identified for NPF in the area:

1. SO_2 ~~SO_2~~ arriving at the site appears to trigger nucleation and growth events.
2. VOC availability (monoterpenes and isoprene) enhances nucleation and growth.
3. The hours with high VOCs concentrations and higher oxidation capacity in the atmosphere (OH concentrations are assumed to be higher during the hours with higher PAR) have higher particle number concentrations and generally guaranteed growth up to the accumulation mode.
4. Growth without the influence of SO_2 ~~SO_2~~ may occur but will do so at a slower rate.

During most of the daytime events SO_2~~SO_2~~ and NO_2 ~~NO_2~~ plumes impacted the site at some stage of each event.

On some occasions the SO_2 ~~SO_2~~ plume might last for a couple hours as shown in the first part of the event on Feb 11th 2020 (see Figure 2~~Figure 2~~~~Figure 2~~), whilst at other times there were multiple peaks of high SO_2 ~~SO_2~~ measured at the site as shown in several other events in the record (e.g. Figures S2, S3, S4). However, subsequent nucleation was observed on every occasion that SO_2~~SO_2~~ was observed above the detection limit at the ~~site, growth~~site, growth occurred within 0 to 150 minutes after the SO_2~~SO_2~~ was first detected. The time window difference between events reflects the influence of conditions at the start of a particle growth event. To highlight this phenomenon a cross correlation between SO_2 ~~SO_2~~ and the aerosol mass of aerosol SO_4^{2-} ~~SO_4~~ time series obtained from the tof-ACSM and the measured particle number concentration (CN_3) was applied. Figure 4~~Figure 4~~~~Figure 4~~ shows the Pearson correlation between SO_2~~SO_2~~ and the CN_3 and aerosol SO_4^{2-} in a window period of four hours i.e. starting two hours before the nucleation commenced and ending after the first two hours of the event. This time window captures the SO_2~~SO_2~~ influence on the particle formation. Each line/point shows the correlations at 0, 30, 60, 90, 120 and 150 minutes lagged for each daytime event. The dotted blue lines show where the lagged correlation is significant at ($|r| > 0.5$).

Formatted: Subscript
Formatted: Subscript
Formatted: Superscript
Formatted: Subscript
Formatted: Subscript
Formatted: Not Superscript/ Subscript
Formatted: Font: (Default) +Body (Calibri), 12 pt, Font color: Auto
Formatted: Justified
Formatted: Superscript

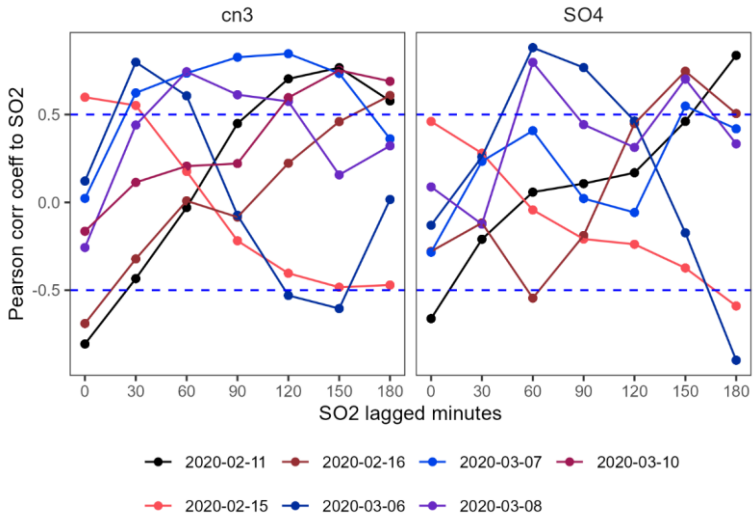

Figure 4 : Pearson correlation values obtained from the cross correlation between SO_2 and CN_3 and SO_4^{2-} mass. The dashed lines represent the 0.5 threshold as a reference to identify significant correlations. Events on Feb 10th and March 11th did not follow this pattern and were removed from the plot.

To interpret Figure 4~~Figure 4Figure 4~~, we can use the event on February 11th (black line) as an example. Here the correlation between SO_2 ~~SO_2~~ and CN_3 becomes significant (at $|r| > 0.5$) if the SO_2 time series is lagged 120 minutes with respect to the aerosol data; and the correlation between SO_2 ~~SO_2~~ and aerosol SO_4^{2-} ~~SO_4^{2-}~~ becomes significant after 3 hours. This means that if we move the SO_2~~SO_2~~ time series two hours forward it will be better correlated with the particle number concentration, accounting for the reaction time of SO_2~~SO_2~~ to produce H_2SO_4~~H_2SO_4~~ and enhance/trigger the particle formation under the conditions in the atmosphere at the time. Usually, the SO_2 correlation with aerosol SO_4^{2-} ~~SO_4^{2-}~~ needs a longer lag time to be significant. This is a potential indication of the order in which the chemical reactions happen. First, we will see oxidation of the SO_2 ~~SO_2~~ to H_2SO_4~~H_2SO_4~~ then nucleation, and finally growth in mass when there is condensation or coagulation near CCN sizes. Using time series analysis as shown here can provide more evidence when the chemical mechanisms are known but observations of other variables are not available.

A similar result is observed for other events at different lagged times. The difference in the time necessary to achieve a significant correlation between SO_2 ~~SO_2~~ and the particle number seems to be related to the quantity of VOCs available when the SO_2 ~~SO_2~~ plume arrives at the site. This aligns with our understanding of the transition from nucleation to particle growth. In the early hours, observed monoterpene levels are sufficient to drive nucleation through ozonolysis and subsequent HOM formation~~This matches our understanding of the process from nucleation to particle growth, at early hours we observed monoterpenes~~

Formatted: Superscript

Formatted: Superscript

Formatted: Caption

Formatted: Font: (Default) +Body (Calibri), 12 pt, Font color: Auto

~~levels that are sufficient to promote nucleation through ozonolysis and HOM formation~~ (Iyer et al., 2021; Kirkby et al., 2023; Wang et al., 2023). Particle growth was observed later in the day (see Figure 2 for example) likely driven by the condensation of OVOCs. The increase in the sulfate fraction observed in the ACSM supports the condensation of sulfate-related species onto the growing particles. Events on February 15th, March 6th, and March 7th showed the highest correlations within the first 30 minutes of lagging the data. Common to these events were relatively high levels of monoterpenes (~1 ppb either directly observed or inferred from high PAR and temperature) in the hour before NPF detection at the site (see Figure S1, S2, and S4). The elevated monoterpene levels and subsequent ozonolysis likely initiated particle formation during these times, with available H_2SO_4 further facilitating nucleation. The ~~but potentially not enough to promote growth to larger sizes as it seems most of the particle growth observed could be related to isoprene levels. Later with higher temperatures, emissions of isoprene increase so that ELVOC or other OVOCs are potentially produced that contribute to growth in particle mass reflected in the increase of the sulphate fraction observed in the ACSM. Events on February 15th, March 06th and March 07th showed highest correlations in the first 30 minutes of lagging the SO_2 data. Common to all these events was a relatively high isoprene mole fraction and enhanced levels of monoterpenes (~1 ppb) in the hour before SO_2 being detected at the site (see Figure S1, S2 and S4) or in the circumstances where VOC data were not available, conditions where isoprene and monoterpenes mole fractions were assumed to be high by associated with weather conditions (i.e. high PAR and temperature see Figure S5). The high levels of monoterpenes and subsequent ozonolysis could be driving the particle formation at these times. In this period H2SO4 is available to drive the nucleation and the~~ HOM proxy (monoterpenes*ozone (e.g.: Zhang et al., 2024)) also peaked during this period, supporting the idea that HOM formation via ozonolysis was a dominant oxidation pathway driving initial nucleation. ~~at it's highest values during the day potentially enhancing the effect.~~

The event on March 8th also met this condition (see Figure 5~~Figure 5~~~~Figure 5~~), although it exhibited a relatively low growth rate. Elevated isoprene and MACR + MVK concentrations during this event suggest the potential for isoprene to suppress new particle formation, as described by~~although the event showed a relatively low growth rate. The isoprene and MACR + MVK concentrations in this event highlight the possibility of isoprene suppression~~ (Heinritzi et al.~~,~~ (2020). Higher isoprene levels after 12:00, accompanied by increased MACR + MVK coincided with a decline in the number of smaller particles (although CN_3 data is incomplete). ~~The higher isoprene levels after 12:00, along with the increase of MACR +MVK indicate isoprene oxidation through OH.~~ This is the first step in the reaction chain to produce C_{15} dimers. This observation aligns with the HOM proxy (monoterpenes*ozone): higher proxy values corresponded to periods of higher particle numbers, while a decrease in the HOM proxy coincided with a decrease in particle numbers and an increase in MACR + MVK products, suggesting a shift towards ~~a~~ more isoprene-influenced atmospheric chemistry. Concurrently, increases in the organic and sulfate fractions, along with the condensation sink, indicate a shift towards conditions favoring the growth of existing larger particles through condensation and coagulation, rather than ~~new~~ nucleation events.~~Although the CN_3 data is not complete for the event, it is clear there was a decline of the number of particles in the smaller sizes at the same time as the oxidation products of isoprene increase. This is also supported using the HOM formation proxy (monoterpenes*ozone), where at the times with higher particle numbers, the HOMS proxy is higher and then when the particle number decreases the HOM proxy does it too while MACR+MVK products increase~~

Formatted: Font: (Default) +Body (Calibri), 12 pt, Font color: Auto

Formatted: Superscript

Formatted: Superscript

Formatted: Superscript

Formatted: Font: (Default) +Body (Calibri), 12 pt, Font color: Auto, English (Australia)

Formatted: Subscript

Formatted: Subscript

~~suggesting a change to a more isoprene driven chemistry. The organic and sulphate fraction increase as well as the condensation sink suggesting larger particle formation and conditions that favour condensation and coagulation instead of nucleation.~~

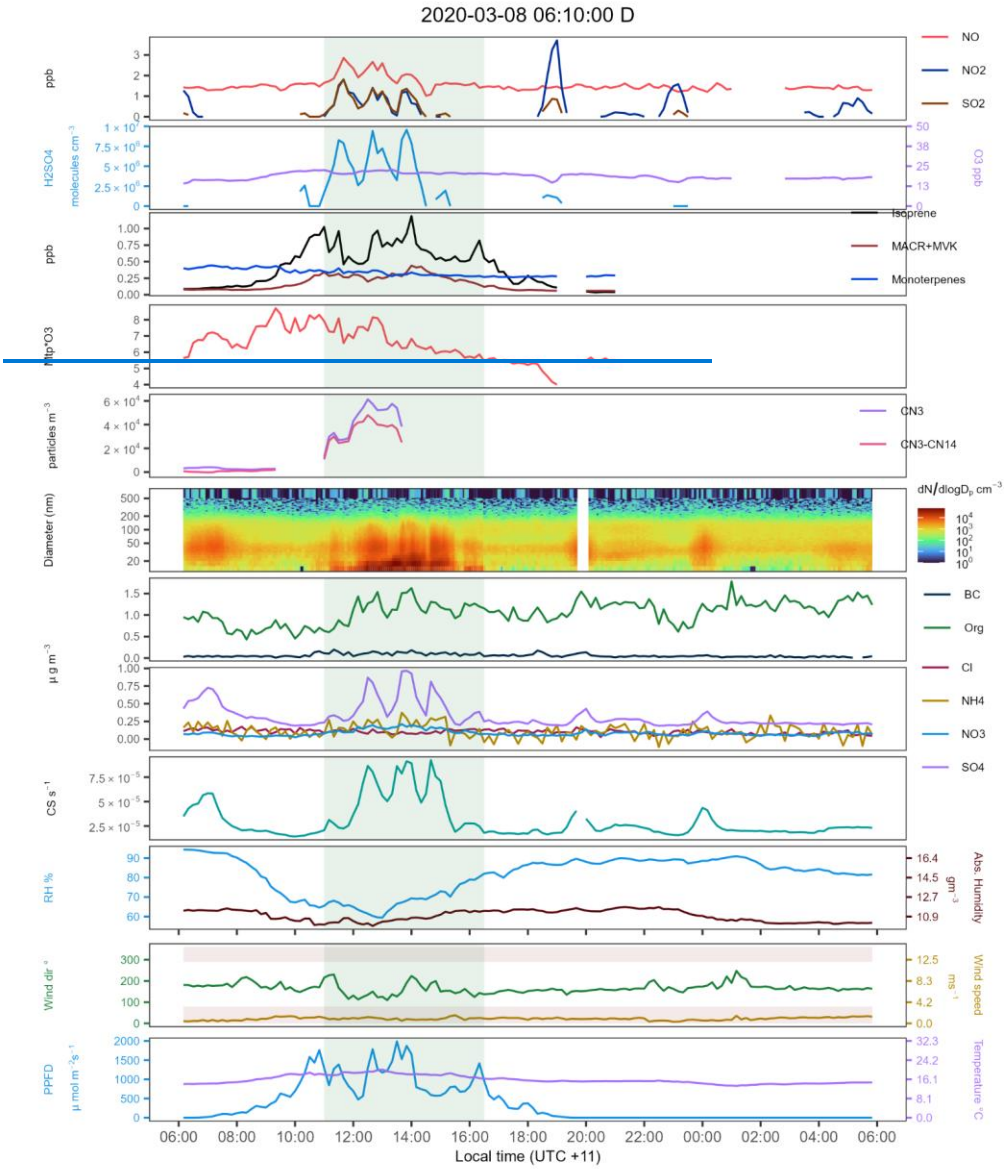
2020-03-08 06:10:00 D
NO
NO2
SO2
ppb
H2SO4
molecules cm⁻³
O3 ppb
Isoprene
MACR+MVK
Monoterpenes
Mtp*O3
particles m⁻³
CN3
CN3-CN14
Diameter (nm)
dN/dlogDp cm⁻³
BC
Org
Cl
NH4
NO3
SO4
μ g m⁻³
CS s⁻¹
RH %
Abs. Humidity
gm⁻³
Wind dir °
Wind speed
ms⁻¹
PPFD
μ mol m⁻²s⁻¹
Temperature °C
06:00
08:00
10:00
12:00
14:00
16:00
18:00
20:00
22:00
00:00
02:00
04:00
06:00
Local time (UTC +11)

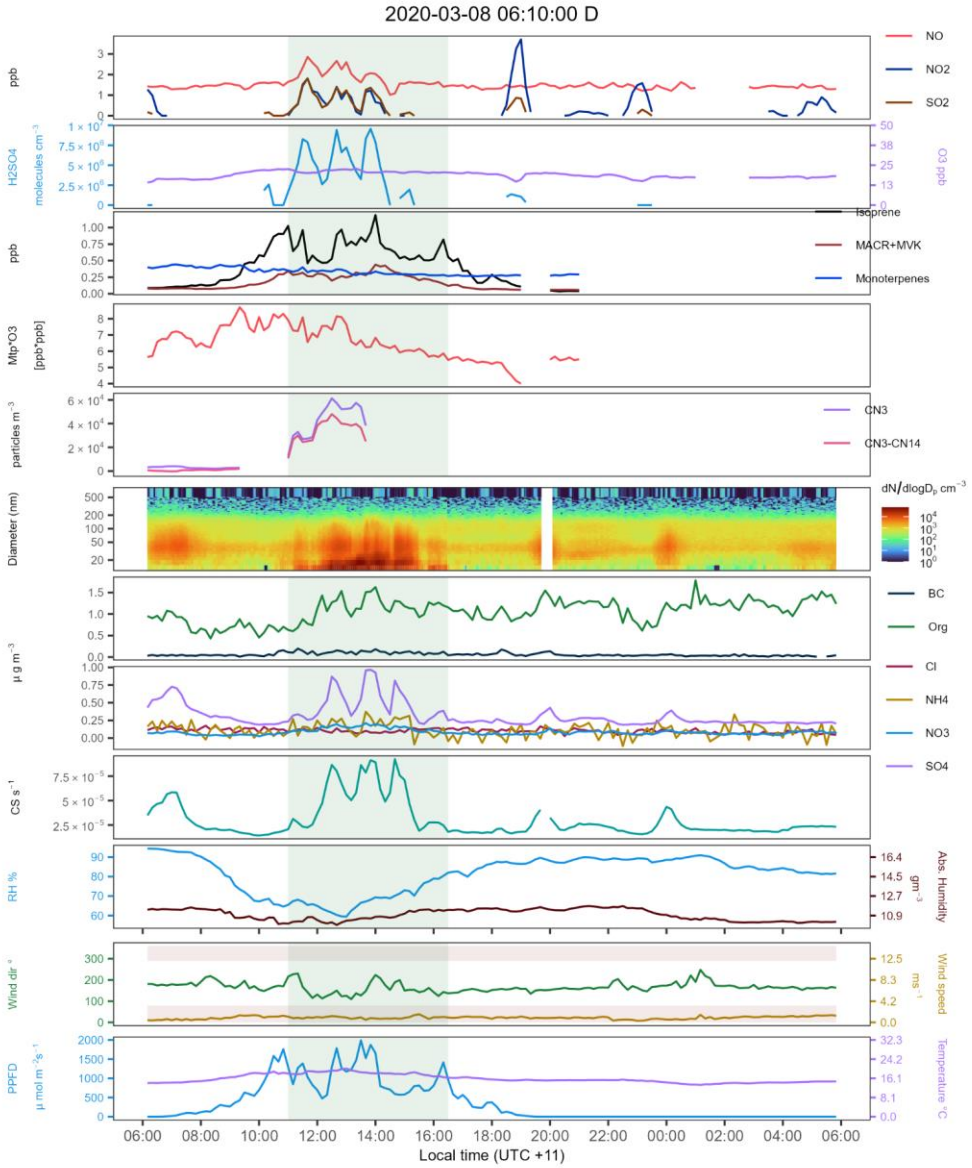

Figure 5 Time series of all selected variables during the NPF event during 2020-03-08. NO = Nitric oxide, NO_2 = Nitrogen dioxide, SO_2 = Sulphur dioxide, H_2SO_4 = Sulphuric acid, O_3 = Ozone, MACR+MVK = isoprene ox. products methacrolein and methyl-vinyl-ketone, CN_3 = Condensation

Formatted: Subscript
Formatted: Subscript
Formatted: Subscript
Formatted: Subscript
Formatted: Subscript
Formatted: Subscript

*Nuclei >3nm, CN_3-CN_{14} = difference of CN_3 minus the sum of all channels from the SMPS data. BC = Black carbon. Org = Organic mass fraction, NH_4 = Ammonium mass fraction, NO_3 = Nitrates mass fraction, SO_4^{2-} = Sulphates mass fraction, Cl = Chloride mass fraction. CS = condensation sink. Mtp*ozone = HOM proxy product monoterpenes and ozone [ppb*ppb].*

The Feb 11th and Feb 16th events had similar arrival times for the SO_2 ~~SO_2~~ pollution (8:00 to 9:00) although the photochemistry was not fully active yet (see H_2SO_4), monoterpenes levels were consistently high during all the campaign (~0.4 ppb based on the days with data), enough to promote nucleation. This presumption is supported by looking at the event on February 16th (see Figure S3). In this event, a first peak of SO_2 ~~SO_2~~ at 8:00 started nucleation but then condensation or coagulation dominated favouring growth. The CN_3 -CN_{14} data show that after that initial nucleation period the particle number is dominated by the >14nm fraction. Multiple SO_2 ~~SO_2~~ plumes ~~came to site~~reaching the site ~~producing~~ produced higher ratios of H_2SO_4, but ~~it~~ promoted growth to larger particles sizes particularly on the sulphates fraction that correlates with the SO_2 ~~SO_2~~ peaks. In the evening there were a couple of small particle bursts that were quickly coagulated on larger size particles.

~~The event on~~On March 10th ~~–~~(see ~~Figure 6Figure 6Figure 6~~)~~–~~, a sharp decline in high monoterpene concentrations was observed just before the aerosol event. The aerosol growth phase is then observed to correlate with peaks in SO_2 and NO_X, as well as elevated levels of isoprene. This suggests monoterpene ozonolysis initiated nucleation, and the observed particle growth coincided with periods indicative of increased atmospheric pollution, potentially contributing condensable material.~~shows high monoterpene concentrations that declined quickly just prior to the event being observed in the aerosol data. The aerosol growth phase is then observed to correlate with peaks in SO_2 and NO_X, as well as elevated levels of isoprene. Together, this suggests monoterpene ozonolysis initiated nucleation, followed by condensational growth via isoprene oxidation products.~~

406 **Formatted:** Subscript
407 **Formatted:** Subscript
408 **Formatted:** Subscript
409 **Formatted:** Subscript
410 **Formatted:** Subscript
411 **Formatted:** Subscript
412 **Formatted:** Superscript
413
414
415
416
417
418
419
420 **Formatted:** Superscript
421 **Formatted:** Font: (Default) +Body (Calibri), 12 pt, Font color: Auto
422
423 **Formatted:** Subscript
424 **Formatted:** Subscript
425
426
427
428

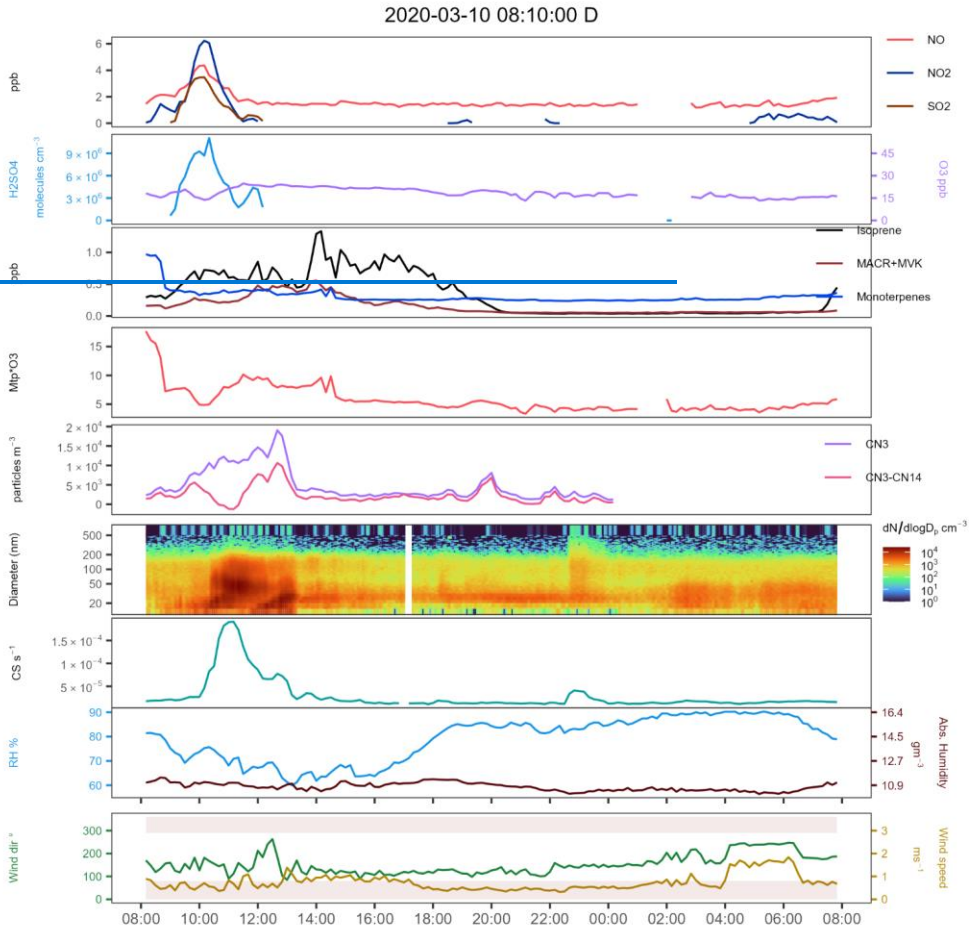
2020-03-10 08:10:00 D
ppb
NO
NO2
SO2
H2SO4
molecules cm^{-3}
O3 ppb
Isoprene
MACR+MVK
Monoterpenes
Mtp*O3
particles m^{-3}
CN3
CN3-CN14
Diameter (nm)
dN/dlogD$_p$ cm^{-3}
CS s^{-1}
RH %
Abs. Humidity
gm^{-3}
Wind dir °
Wind speed
ms^{-1}
08:00
10:00
12:00
14:00
16:00
18:00
20:00
22:00
00:00
02:00
04:00
06:00
08:00

429

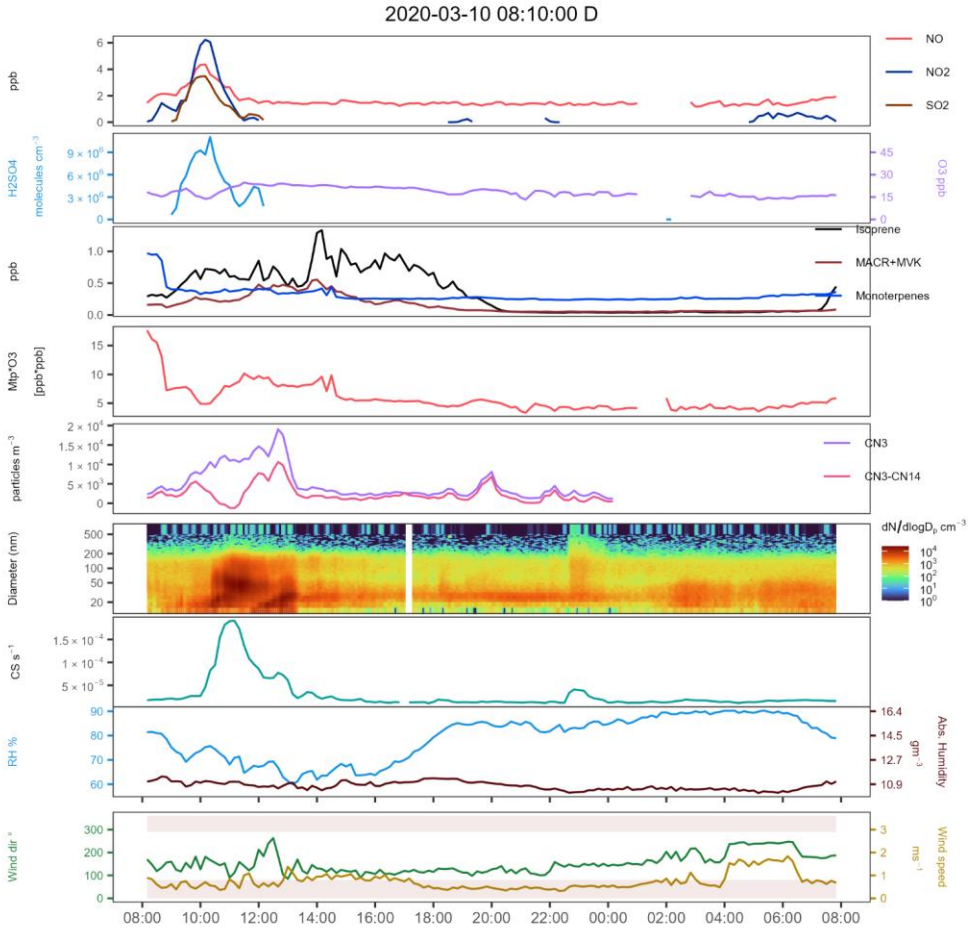

*Figure 6 Time series of all selected variables during the NPF event during 2020-03-10. The drop of CN_3 seem related to the lack of SO_2 after 11:00. NO = Nitric oxide, NO_2 = Nitrogen dioxide, SO_2 = Sulphur dioxide, H_2SO_4 = Sulphuric acid, O_3 = Ozone, MACR+MVK = isoprene ox. products methacrolein and methyl-vinyl-ketone, CN_3 = Condensation Nuclei >3nm, CN_3-CN_{14} = difference of CN_3 minus the sum of all channels from the SMPS data.. CS = condensation sink. Mtp*ozone = HOM proxy product monoterpenes and ozone [ppb*ppb]. ~~NO = Nitric oxide, NO2 = Nitrogen dioxide, SO2 = Sulphur dioxide, H2SO4 = Sulphuric acid, O3 = Ozone, MACR+MVK = isoprene ox. products methacrolein and methyl-vinyl-ketone, CN3 = Condensation Nuclei >3nm, CN3-CN14 = difference of CN3 minus the sum of all channels from the SMPS data. CS = condensation sink. Mtp*ozone = HOM proxy product monoterpenes and ozone [ppb*ppb].~~*

For all ~~date day time~~daytime events SO_2 ~~SO_2~~ and NO_2~~NO_2~~ are significantly correlated with a Pearson correlation of 0.78, suggesting a common source for both pollutants. The closest source of combustion products is the Appin Road located north of the sampling site. Given that the sampling site is away from other possible sources of SO_2~~SO_2~~ and NO_2~~NO_2~~ and the relatively low wind speeds during most of the campaign (see Figure S~~6~~8), combustion from mobile sources is considered the most likely source of both compounds but there might be some influence of more distant coal-fired power stations. Another factor to contribute to this theory is that the SO_2 ~~SO_2~~ levels were higher during the day when most of the commuting takes place and leading to a higher vehicle density on the roads. The intermittent SO_2~~SO_2~~ and NO_2~~NO_2~~ peaks suggest the influence of mobile sources with poor emission control onboard. The effects of vehicles with poor emission control technologies on ambient concentrations of SO_2, NO_x , AVOCs and PM has been seen in different studies (Kari et al., 2019; Phillips et al., 2019; Smit et al., 2019) and the legislation controlling fuel standards and emissions is relatively lax in New South Wales (Paton-Walsh et al., 2019).

During the COALA-2020 campaign, many events, such as the one on February 16th (Figure S3), exhibited elevated gas-phase SO2. The availability of ~~M~~monoterpene to ~~availability for~~ form~~ing~~ highly condensable ULVOC/ELVOC is crucial in the observed events. While the oxidation products of isoprene can also condense on pre-existing particles (Stangl et al., 2019), the dominant pathways and their efficiency are likely driven by monoterpenes. ~~During the COALA-2020 campaign, many events, such as the one on February 16th (Figure S3), exhibited elevated gas-phase SO2.~~ Although VOC data was not available for February 16th, the consistent diurnal profile of VOCs observed throughout the remaining dataset (Figure S5) suggests enhanced monoterpene and isoprene availability during the daytime. Under these conditions of available BVOCs, particle growth was frequently observed, suggesting a contribution from condensed organic material. As the night approaches and BVOC emissions decrease with temperature, the remaining OVOCs can undergo further oxidation, forming less volatile species that are more prone to condensation on existing particles. However, the limited availability of VOCs after their consumption (estimated around 22:00 based on diurnal cycles in Figure S5) likely restricts further growth~~The atmospheric availability of monoterpenes to react and produce ULVOC or ELVOC with higher condensation potential to existing $SO_4^=$ aerosol is as important as the SO_2 presence and reaction, as seen in most of the events. Isoprene oxidation products also have a role in condensing on pre-existing nucleated aerosol. This has been previously reported by (Stangl et al., 2019), where chamber experiments showed that SO_2 presence can significantly enhance SOA formation from isoprene and monoterpene oxidation by ozone. Xu et al (2021b) reported that water and SO_2 availability will change the role of SO_2 in the particle formation process. With high SO_2 mole fractions, the SO_2 reaction path will favour reaction to peroxides instead of stable Criegee intermediates, thereby enhancing particle growth, particularly at relative humidity of greater than 45%; a condition present during most of the COALA-2020 campaign. This suggests that under high SO_2, isoprene and monoterpene availability, and high relative humidity conditions, particle formation and eventual growth is likely to occur.~~

~~Such an effect was observed in some of the events, for example the event on February 16th (Fig S3). This event saw high relative humidity throughout the event (well above the 45% threshold suggested by Xu et al.) as well as elevated gas-phase SO_2. Unfortunately VOC data wasn't available during this event, however the consistent diurnal profile of VOCs observed throughout the remaining dataset (Figure S5)can be extrapolated to this day, suggesting enhanced monoterpene and isoprene availability. Together, these prerequisites were met, and likely led to the observed aerosol growth event.~~

Formatted: Font: Not Bold

Formatted: Superscript

Formatted: Superscript

~~The conditions promoting sulphate formation in the event of Feb 16th are also present in multiple events. As the night approaches, BVOC emissions decrease with temperature, leaving all existing VOCs to oxidize. This provides the initiation for further oxidation of OVOCs into more oxidized species, which are more likely to condense on existing particles. In addition, with the temperature decreasing the relative humidity increases, making this the ideal condition for particle growth, particularly sulphates. However, once the VOCs are mostly consumed (assumed from diurnal cycles from the campaign to be around 22:00, see figure S5), there are insufficient VOCs to promote growth. This relationship is presented in Figure 7, where relative humidity and sulphate mass are positively correlated during the afternoon hours in the events which had multiple SO_2 peaks enhancing sulphate formation and particle growth.~~

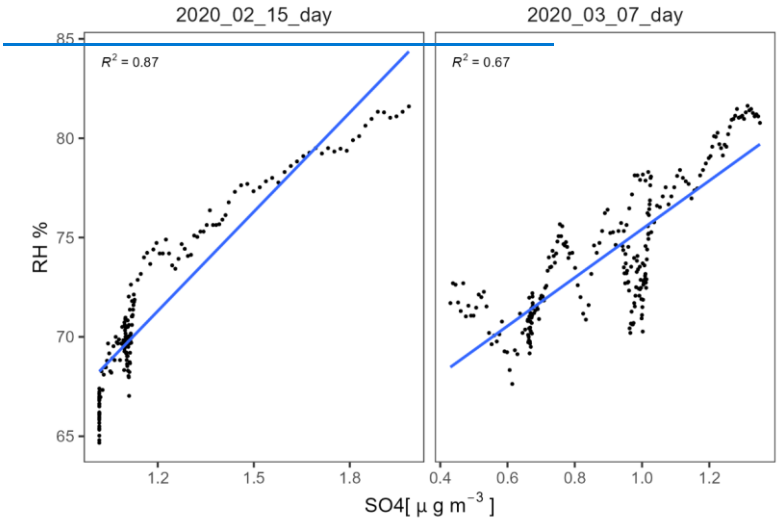

~~Figure 7: Scatter plot of the events on Feb 15th and March 7th comparing total sulphate mass against relative humidity in the afternoon hours (14:00 to 17:00).~~

When there is negligible SO_2 in the atmosphere but high VOC concentrations (particularly monoterpenes), autooxidation processes can be initiated, potentially leading to both nucleation and subsequent particle growth (Bianchi et al., 2019). Growth was observed during the first event on February 10th (see daytime data in Figure 7) despite low SO_2 and may be related to the condensation of HOMs formed through monoterpene autooxidation. The average concentration of monoterpenes during the campaign in the morning was often sufficient to initiate reactions leading to ULVOC that favor both new particle formation and the growth of pre-existing particles. ~~When there is negligible SO_2 in the atmosphere but there are high enough VOC concentrations, there can be particle growth when dimers C_{15} produced by further OH oxidation of isoprene products, condensate over smaller particles (Heinritzi et al., 2020). Growth was observed during the first event on February 10th (see daytime data in Figure 8) and may be related to the condensation of these~~

Formatted: Body Text

Formatted: Subscript

Formatted: Superscript

Formatted: Font: (Default) +Body (Calibri), 12 pt, Font color: Auto, English (United States)

Formatted: Subscript

~~dimers. The average concentration of isoprene during the campaign in the morning is higher than 1 ppb, enough to initiate the reactions leading to LVOCs favouring growth of preexisting particles.~~

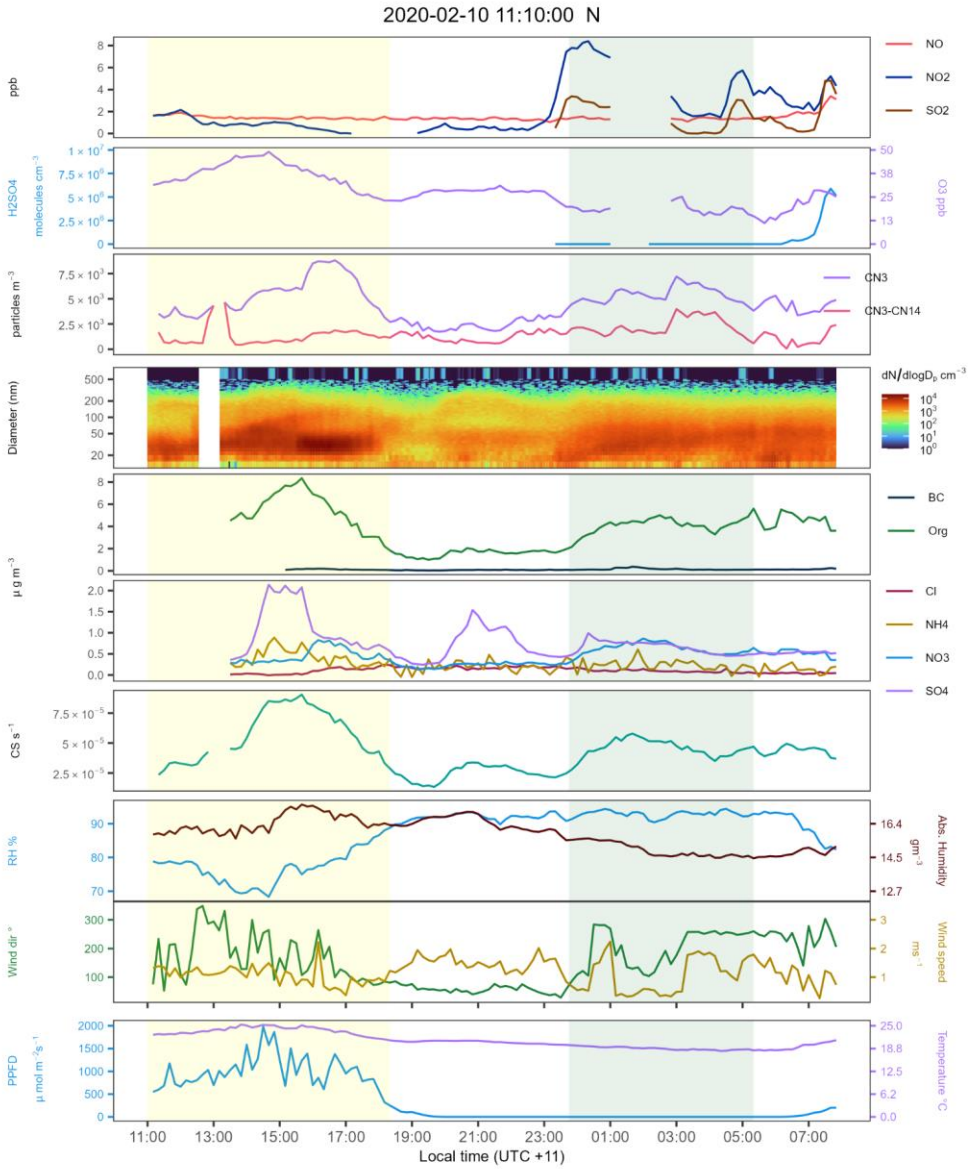

Figure 7~~8~~: Time series for all selected variables during the NPF event during 2020-02-10~~-~~. NO = Nitric oxide, NO_2 = Nitrogen dioxide, SO_2 = Sulphur dioxide, H_2SO_4 = Sulphuric acid, O_3 = Ozone, CN_3 = Condensation Nuclei >3nm, CN_3-CN_{14} = difference of CN_3 minus the sum of all

*channels from the SMPS data. BC = Black carbon. Org = Organic mass fraction, NH_4 = Ammonium mass fraction, NO_3 = Nitrates mass fraction, SO_4^{2-} = Sulphates mass fraction, Cl = Chloride mass fraction. CS = condensation sink. Mtp*ozone = HOM proxy product monoterpenes and ozone [ppb*ppb]. NO = Nitric oxide, NO2 = Nitrogen dioxide, SO2 = Sulphur dioxide, H2SO4 = Sulphuric acid, O3 = Ozone, CN3 = Condensation Nuclei >3nm, CN3-CN14 = difference of CN3 minus the sum of all channels from the SMPS data. BC = Black carbon. Org = Organic mass fraction, NH4 = Ammonium mass fraction, NO3 = Nitrates mass fraction, SO4 = Sulphates mass fraction, Cl = Chloride mass fraction, CS = condensation sink. PFFD = Photosynthetic Photon Flux Density VOCs mole fractions were not available during this specific event. Note how there does not seem to be any significant SO_2 or NO_2 pollution prior to the NPF start. At the same time of the particle growth there are enhancements in the organic, sulphate and ammonium mass fraction. There are two events in this plot. One in the morning with an unknown start and ending around 18:00, and the other at night. The light green area marks the night event, and the yellow highlight refers to the daytime event.*

Australia experiences an isoprene-dominated atmosphere ~~The availability of monoterpenes increases the likelihood of NPF before or after SO_2 is available in the atmosphere. Although monoterpenes are quickly oxidized by OH resulting in relatively short lifetimes compared to isoprene (Atkinson, 2000; Atkinson and Arey, 2003), the ozone levels observed during the campaign are enough to promote ozonolysis and nucleation when there is no OH competing.. Australia experiences an isoprene dominated atmosphere~~ (Emmerson et al., 2016; Ramirez-Gamboa et al., 2021)~~, so~~and the chemical balance in the atmosphere can rapidly change, particularly in the hotter seasons when more isoprene is emitted. While SOA formation on pre-existing particles can involve molecules with relatively high saturation vapor pressures, new particle formation critically depends on molecules with extremely low saturation vapor pressures due to the Kelvin effect (Tröstl et al., 2016). ~~(~~Heinritzi et al.~~,~~ (2020) showed that reducing C_{20} formation (α-pinene oxidation in isoprene presence) to favor C_{15} formation reduces nucleation rates. However, it is also important to highlight that C_{15}, C_{10}, and even C_5 oxidation products from isoprene oxidation can contribute to SOA mass on existing particles. Therefore, in Australia's isoprene-dominated environment, higher isoprene to monoterpene ratios could lead to a greater production of C_5 and C_{15} products that contribute to particle growth on existing aerosols (and SOA mass), while simultaneously hindering new particle formation by reducing the formation of C_{20} dimers from monoterpenes.~~so the chemical balance in the atmosphere can rapidly change, particularly in the hotter seasons when more isoprene is emitted. Isoprene oxidises mainly through the OH pathway to more stable compounds; usually MACR and MVK are used as tracers to determine which path and under what conditions isoprene is oxidised. MACR is oxidised to heavier OVOCs that eventually condense and promote SOA formation in the larger sizes but these compounds also suppress NPF (Heinritzi et al., 2020; Link et al., 2021) as previously discussed in the event in Figure 5.~~

3.5 Night-~~time NPF~~time NPF Events

We observed three nighttime events during COALA. Unfortunately, none of these events coincided with all data sets being collected which limits our ability to discuss the reactions driving the nighttime events. Consistent between all nighttime events is an increase in particles (CN_3), elevated NO_2, and an increasing condensation sink. ~~The main factors influencing the night-time events are ozone and NO_x pollution, however the data available for this study does not provide enough information to make a more definitive statement.~~ Unfortunately, the NO_x~~NO_x~~ instrument available in this study was not ideal for this type of measurement for several reasons: it is not designed to be sensitive to the lowNO_x~~NO_x~~ levels observed in rural areas; it is not capable of separating NO_x ~~NO_x~~ from NO_y~~NO_y~~; and it was set up to calibrate in the night hours between 1:00

Formatted: Font: (Default) +Body (Calibri), 12 pt, Font color: Auto
Formatted: Font: (Default) +Body (Calibri), 12 pt, Font color: Auto
Formatted: Subscript
Formatted: Subscript
Formatted: Subscript
Formatted: Subscript
Formatted: Subscript
Formatted: Subscript
Formatted: Subscript
Formatted: Subscript
Formatted: Subscript
Formatted: Subscript

and 2:00 every day. Nonetheless, during the night-time events the particle size distribution data and the CN_3 data showed particle formation and growth from nucleation to Aitken modes when there were considerable increases of NO_2 ~~NO_2~~ and simultaneous decreases in ozone.

When VOC data are available, monoterpene concentrations were moderate and increased steadily during the event (5th Feb ~~-~~and 9th March). Isoprene was high at the start of the event on 5th Feb, (see Figure 8~~Figure 8~~) however the sudden decrease in isoprene concentration likely coincides with sunset on that day. When aerosol composition data was available (10th Feb) aerosol organic, nitrate and ~~sulfates~~sulphate concentrations increase during the event. When ozone data were available, concentrations decreased slightly during the course of the event. ~~However, PM_1 aerosol mass from the ACSM showed a minimal increase at the same time (e.g. event during night of Feb 5th shown in Figure 8Figure 9). This suggest that there are conditions to initiate the particle formation process but the conditions to increase the size/mass of the particles are not present at these times.~~

The frequency of nocturnal events observed in this study is lower than observed previously at a nearby location (Tumbarumba~~-~~ a eucalypt forest site located 300~~X~~ km to the SE~~NN~~ of Cataract (Suni et al., 2009) ~~during summer 2006~~), where in the summer of 2006, nocturnal NPF events were observed on 32% of the analysed nights, and occurred 2.5 times more frequently than ~~day-time~~daytime events. ~~Simulating the~~Simulating the NPF at ~~Tumbbaruma~~Tumbarumba, ~~(~~Ortega et al. ~~,~~ (~~-~~2012) ~~Ortega et al (2012)~~ was able to reproduce the observations from Tumbarumba by ozonolysis of 13 -carene to initiate nucleation and a-pinene to grow particle diameters. Ozonolysis of limonene was found to ~~contribte~~contribute to both nucleation and aerosol growth. The lower frequency observed in our study may be linked to the apparent initiations of nucleation by NO_2, which ~~noctorunaly~~nocturnally can react with O_3 to form nitrate radicals. ~~NO_3~~ ~~(~~Li et al. ~~,~~ (2024)~~Li et al 2024~~, suggest even trace amounts of NO_3 radicals suppress the NPF.

~~The night time nucleation observed in Figure 7Figure 8 is related to an airmass change and might be the result of a combined effect of monoterpene ozonolysis and subsequent OH production after Crieege intermediates decay (Lester and Klippenstein, 2018). Once the OH is available it can produce H_2SO_4 and enhance the nucleation process. In this case, the increases in organic and sulphate mass shortly after the ozone depletion and the increase in CS indicate a growth in existing particles that is visible in the larger sizes in both particle numbers and mass. CN_3-CN_{14} data suggest that there was some nucleation sporadically happening after the event started, but these particles were rapidly coagulated together with pre-existing larger particles.~~

~~The event on Feb 5th may indicate a combination of different factors at play. First, the monoterpenes and ozone levels could be triggering nucleation as observed during the daytime events, but there is a slight increase in monoterpene concentrations potentially driven by slower wind speeds and less mixing volume at night due to the reduced boundary layer height. Secondly, isoprene is observed to be steadily decreasing during this period. There are no enhancements of MACR+MVK so we could speculate that isoprene may be oxidised by the nitrate radical pathway. This is supported by the slight increase in the Nitrates fraction observed with the ACSM around midnight. Later that day around 4:00 am there is a second burst of small~~

546 **Formatted:** Superscript
547 **Formatted:** Superscript
548 **Formatted:** Superscript
549 **Formatted:** Superscript
550 **Formatted:** Font: (Default) +Body (Calibri), 12 pt, Font color: Auto
551
552 **Formatted:** Font: (Default) +Body (Calibri), 12 pt, Font color: Auto, English (Australia)
553
554 **Formatted:** Font: (Default) +Body (Calibri), 12 pt, Font color: Auto
555 **Formatted:** Font: (Default) +Body (Calibri), 12 pt, Font color: Auto
556
557 **Formatted:** Font: (Default) +Body (Calibri), 12 pt, Font color: Auto
558 **Formatted:** Font: (Default) +Body (Calibri), 12 pt, Font color: Auto
559
560 **Formatted:** Font: (Default) +Body (Calibri), 12 pt, Font color: Auto
561
562 **Formatted:** Font: (Default) +Body (Calibri), 12 pt, Font color: Auto
563
564 **Formatted:** Font: (Default) +Body (Calibri), 12 pt, Font color: Auto, English (Australia)
565
566 **Formatted:** Font: (Default) +Body (Calibri), 12 pt, Font color: Auto, English (Australia)
567 **Formatted:** Font: (Default) +Body (Calibri), 12 pt, Font color: Auto, English (Australia)
568
569 **Formatted:** Font: (Default) +Body (Calibri), 12 pt, Font color: Auto
570 **Formatted:** Font: (Default) +Body (Calibri), 12 pt, Font color: Auto
571
572 **Formatted:** Font: (Default) +Body (Calibri), 12 pt, Font color: Auto
573 **Formatted:** Font: (Default) +Body (Calibri), 12 pt, Font color: Auto, Subscript
574
575 **Formatted:** Font: (Default) +Body (Calibri), 12 pt, Font color: Auto
576
577 **Formatted:** Font: (Default) +Body (Calibri), 12 pt, Font color: Auto
578 **Formatted:** Font: (Default) +Body (Calibri), 12 pt, Font color: Auto, Subscript
579
580 **Formatted** ...
581 **Formatted** ...
582 **Formatted** ...
583 **Formatted** ...
Formatted: Body Text, Left

~~particles that follow the same pattern of monoterpenes/ozone. The monoterpene ozonolysis is also seeing in other night events (see Fig S8-S10).~~

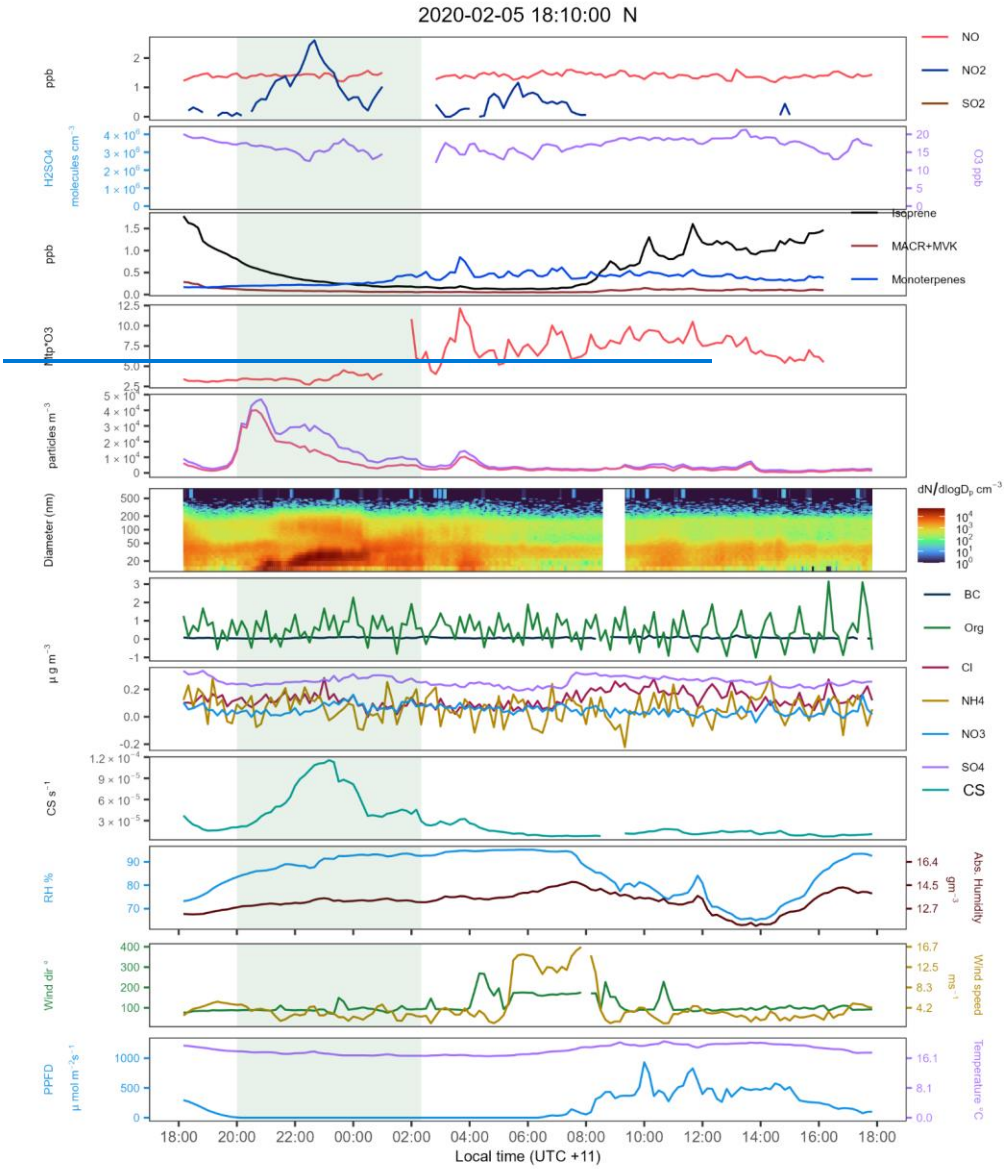
2020-02-05 18:10:00 N
NO
NO2
SO2
ppb
H2SO4
molecules cm⁻³
O3 ppb
Isoprene
MACR+MVK
Monoterpenes
Mtp*O3
particles m⁻³
Diameter (nm)
dN/dlogDp cm⁻³
BC
Org
Cl
NH4
NO3
SO4
CS
μ g m⁻³
CS s⁻¹
RH %
Abs. Humidity
gm⁻³
Wind dir °
Wind speed
ms⁻¹
PPFD
μ mol m⁻²s⁻¹
Temperature °C
18:00
20:00
22:00
00:00
02:00
04:00
06:00
08:00
10:00
12:00
14:00
16:00
18:00
Local time (UTC +11)

586

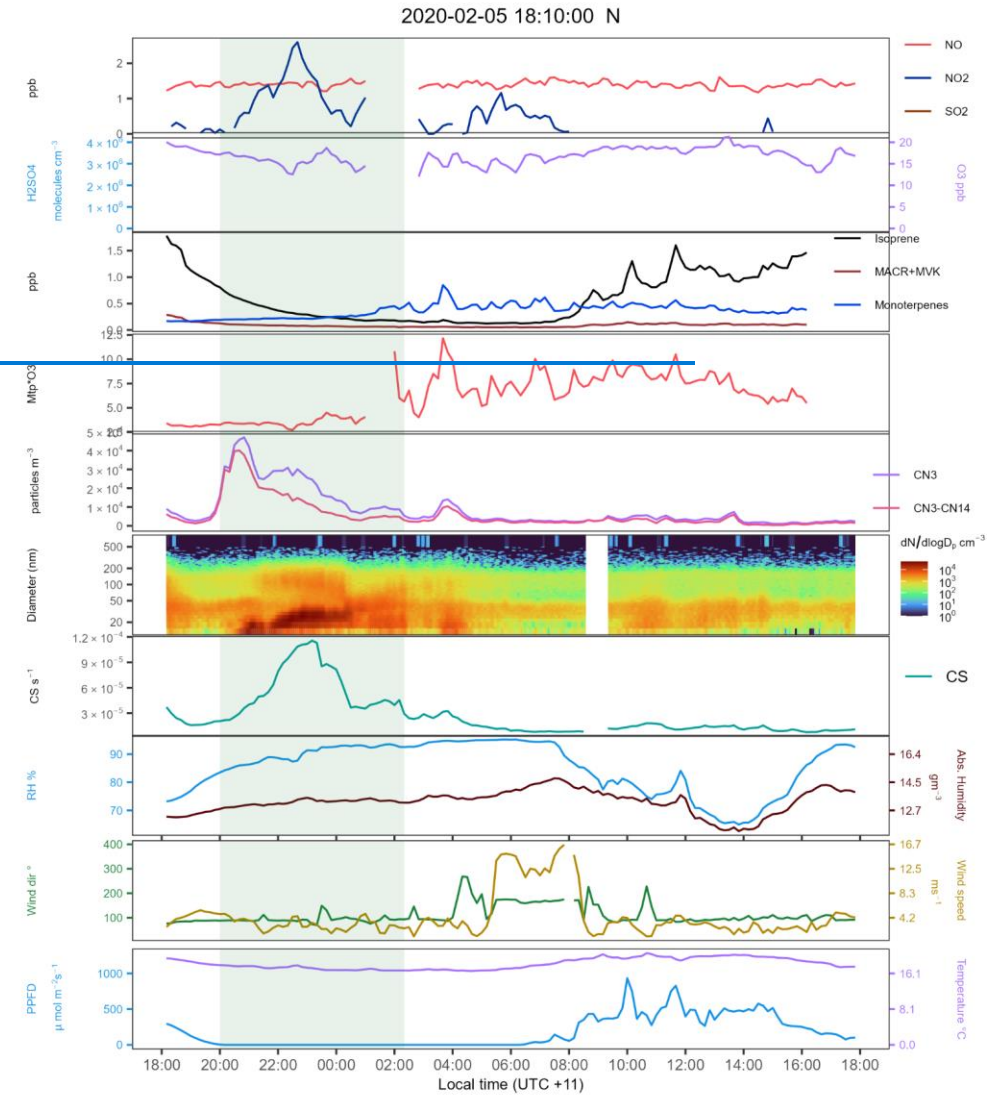
2020-02-05 18:10:00 N
NO
NO2
SO2
ppb
H2SO4
molecules cm^{-3}
O3 ppb
Isoprene
MACR+MVK
Monoterpenes
Mtp*O3
particles m^{-3}
CN3
CN3-CN14
Diameter (nm)
dN/dlogD$_p$ cm^{-3}
CS s^{-1}
CS
RH %
Abs. Humidity
gm^{-3}
Wind dir °
Wind speed
ms^{-1}
PPFD
μ mol m^{-2}s^{-1}
Temperature °C
18:00 20:00 22:00 00:00 02:00 04:00 06:00 08:00 10:00 12:00 14:00 16:00 18:00
Local time (UTC +11)

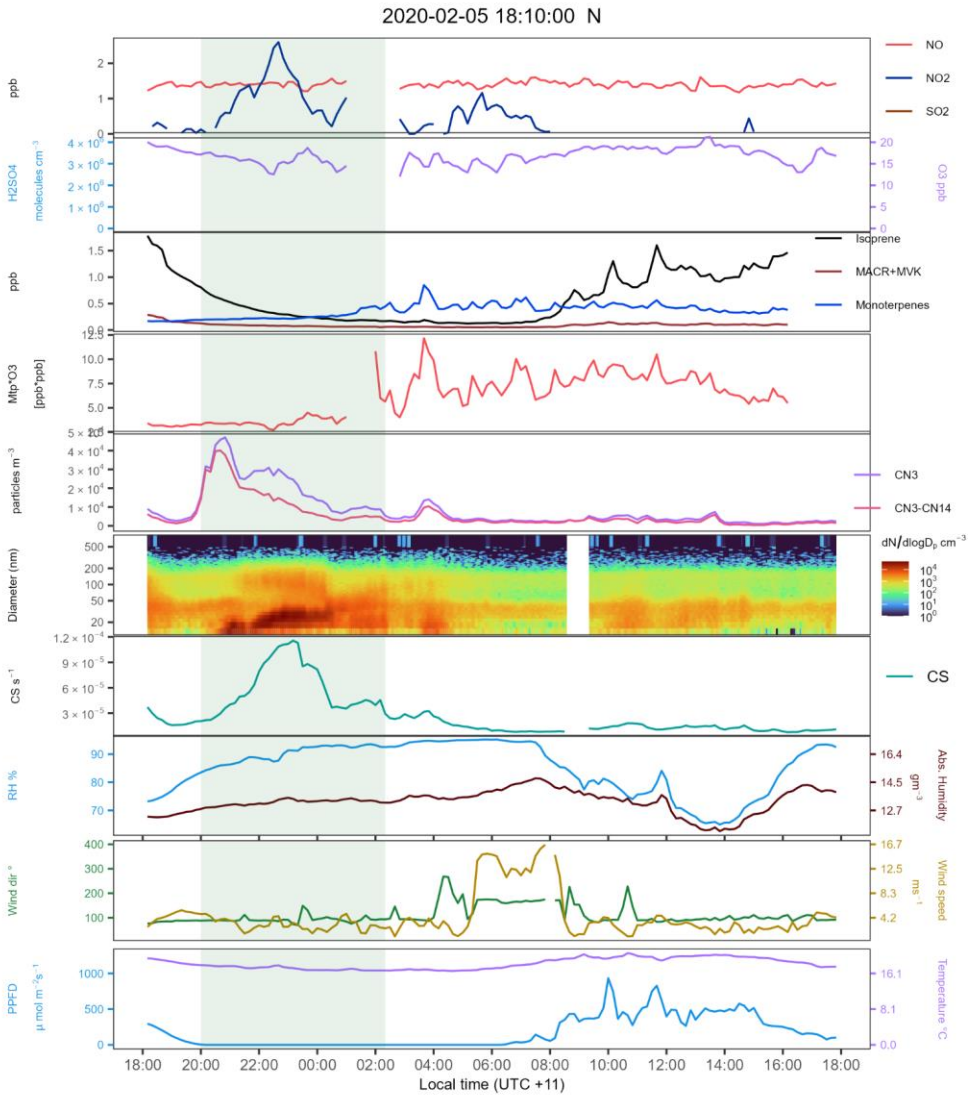

Figure 8~~9~~: Time series for all selected variables during the NPF event during 2020-02-05. NO = Nitric oxide, NO_2 = Nitrogen dioxide, SO_2 = Sulphur dioxide, H_2SO_4 = Sulphuric acid, O_3 = Ozone, MACR+MVK = isoprene ox. products methacrolein and methyl-vinyl-ketone, CN_3 =

Formatted: Subscript
Formatted: Subscript
Formatted: Subscript
Formatted: Subscript
Formatted: Subscript
Formatted: Subscript

*Condensation Nuclei >3nm, CN_3-CN_{14} = difference of CN_3 minus the sum of all channels from the SMPS data. BC = Black carbon. Org = Organic mass fraction, NH_4 = Ammonium mass fraction, NO_3 = Nitrates mass fraction, SO_4 = Sulphates mass fraction, Cl = Chloride mass fraction. CS = condensation sink. Mtp*ozone = HOM proxy product monoterpenes and ozone [ppb*ppb]. Note how the particle number goes below 10000 after the growth reached Aitken mode (0:00). There is not a substantial increase in the aerosol mass when the particle number and geometrical particle diameter increase. The light green area marks the NPF and growth period mentioned in the analysis.*

591 **Formatted:** Subscript
592 **Formatted:** Subscript
593 **Formatted:** Subscript
594 **Formatted:** Subscript
595 **Formatted:** Subscript
Formatted: Subscript

3.6 Aerosol fraction: Day vs Night

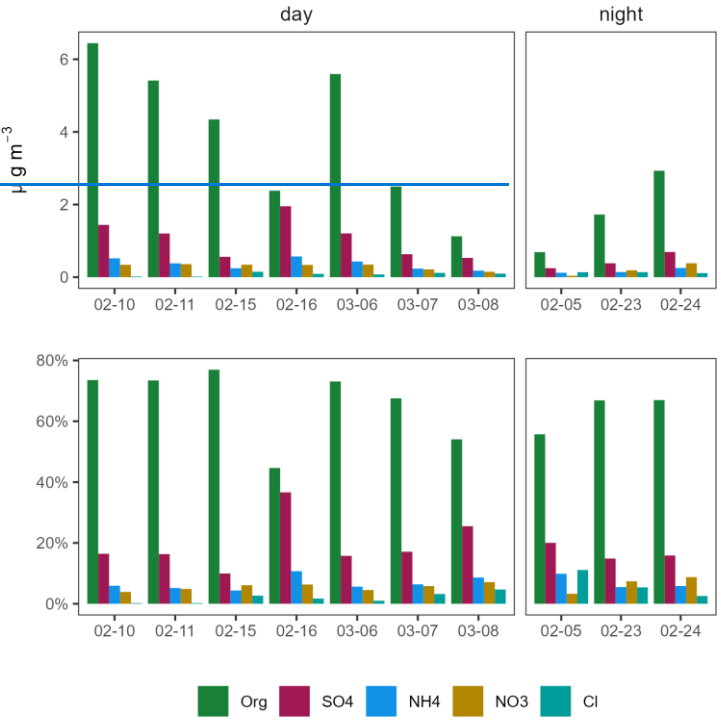

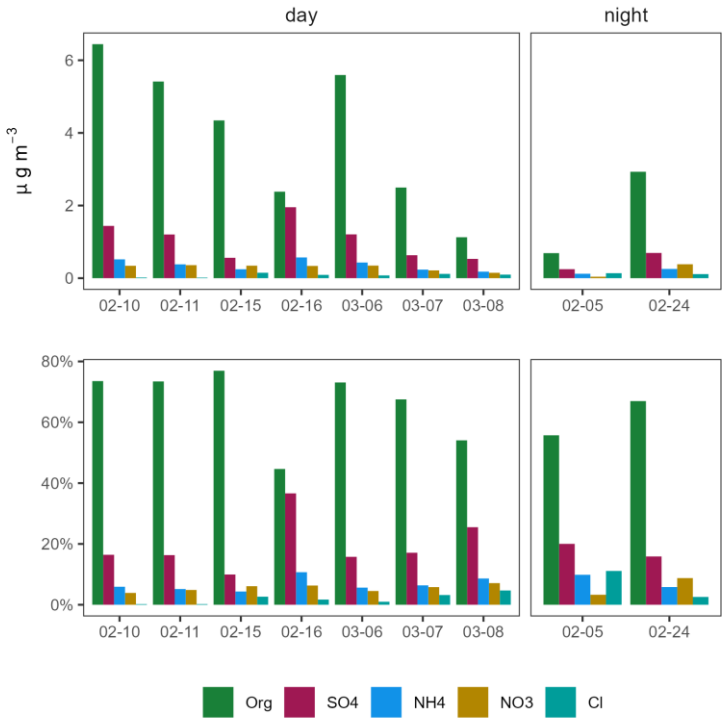

598

Figure 9910: Average mass for each chemical group and event on the top panels. The bottom panel presents the percentage contribution to the mass of each of those fractions based on the average value presented above. Org = Organics; SO_4^{2-} = sulphates; NH_4 = ammonium; NO_3 = nitrates and Cl = chlorides.

599
600
601

Formatted: Font: (Default) Palatino Linotype, 9 pt, Italic, Font color: Text 2, (Asian) Chinese (Simplified, Mainland China), (Other) English (United States)

Formatted: Captioned Figure

Formatted: English (United States)

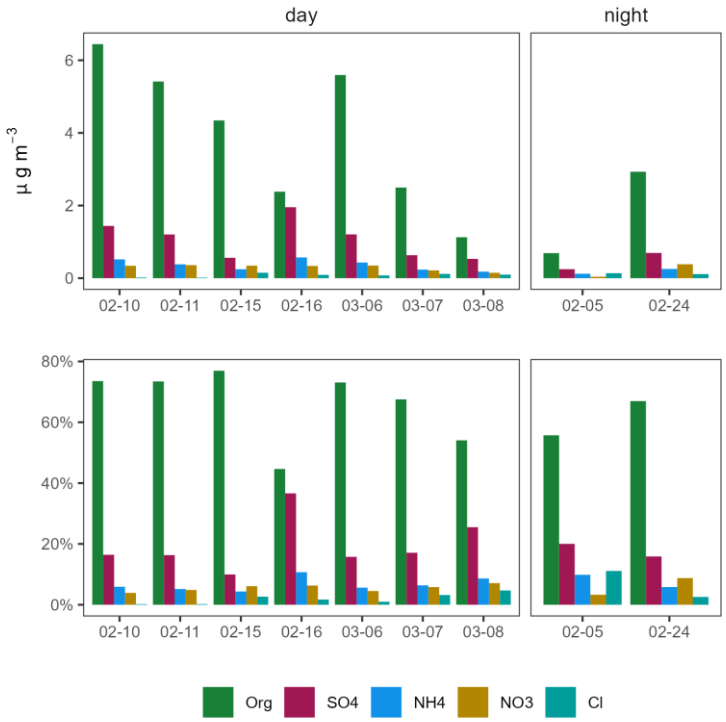

Figure 9~~Figure 9~~Figure 10 shows the mass fraction of the PM_1 aerosol mass ~~as~~ measured in the ACSM. Most of the daytime events show a similar mass fraction distribution. The organic fraction is the largest mass fraction followed by sulphates, ammonium, nitrates, and chlorides. We observed higher sulphate mass fractions in days with higher SO_2 availability such as the events on Feb 16th and March 8th, where the

Formatted: English (United States)

average sulphate mass fraction was larger or similar to the organic fraction (see

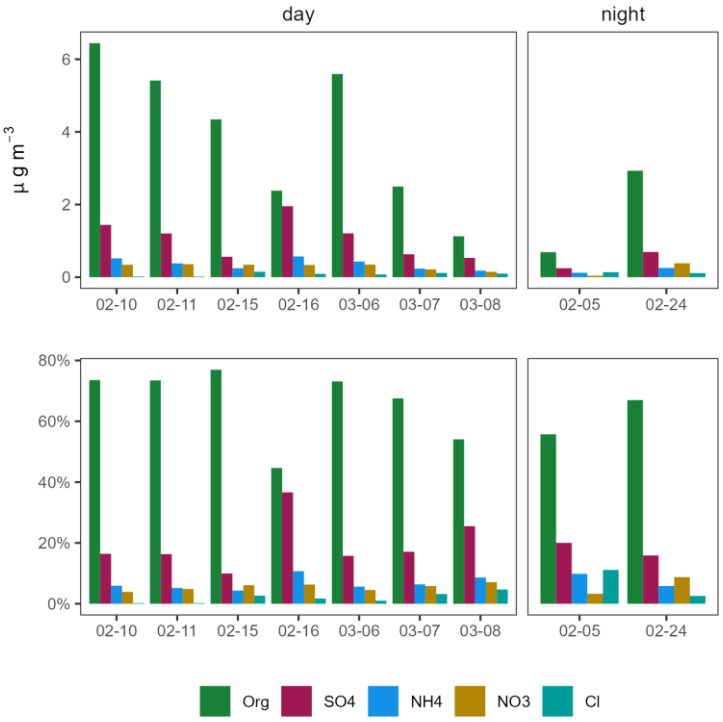

Figure 9~~Figure 9~~Figure 10). These two events also display the highest proportion of ammonium during daytime events. The overall mass during night-time is much lower than during daytime, likely related to the lower concentrations of VOCs available during the night, resulting in growth not reaching sizes where it was detectable by the ACSM. Even with less total mass during the night, the contribution of each fraction is similar to the daytime events. The most notable difference between the mass fractions during day and nighttime NPF events is the higher fraction of chlorides during night-time. Chloride is a primarily sourced aerosol component, so is not influenced by the ~~attributed to a decrease in the~~ aerosol formation capacity of the atmosphere at night that reduces the total organic, sulphate, nitrate and ammonia mass but does not impact chlorides. ~~as much.~~

Something to highlight is the higher fraction of ammonium compared to nitrates through most of the events. Regions with low NO_x have been previously characterized with higher ammonium fractions compared to nitrates (Du et al., 2015; Liu et al., 2022; Petit et al., 2015; Takami et al., 2005; Topping et al., 2004), whilst regions with higher NO_x concentrations favour nitrate formation (Hu et al., 2015; Parworth et al., 2015; Poulain et al., 2020; Schlag et al., 2016). The urban vs rural difference in relative mass composition is evident

Formatted: English (United States)

when comparing this study with the aerosol mass fractions observed in an urban site in Sydney (Keywood et al., 2016) in which high nitrate fractions were observed during most of the campaign.

4. Summary and Conclusions

Here we present aerosol concentration and composition data, VOCs and air pollutant concentrations collected during part of the COALA-2020 campaign including data from 5th Feb to 17th March at a rural site south of Sydney, Australia. This period followed the Black Summer fires after heavy rainfall cleared the smoke, offering insights into atmospheric processes under clean background conditions.

The atmosphere during the sampling period was classified as highly reactive with particle formation identified on more than 3950% of the sampling days. Like previous studies, daytime NPF events coincided with the arrival of anthropogenic plumes at the site, suggesting their role in initiating particle formation. The positive relationship between ~~isoprene~~ monoterpene concentrations and both PM_1 organic aerosol mass and CN_3 suggests a direct relationship between biogenic emissions and organic aerosol formation.

The change between gas to aerosol phase was indirectly analysed through the evaluation of the conditions leading to NPF events. This analysis showed how SO_2 plumes impacting the site drove NPF. The particle growth rate was dependent on available VOCs in the atmosphere and OH availability, also enhanced during periods with higher relative humidity and multiple intrusions of SO_2 and NO_x plumes producing particles larger than 100 nm.

Night-time events were attributed mainly to oxidation with ozone~~, and some potential growth through the isoprene/nitrate radical oxidation pathway.~~ . Although most of the night-time events showed the influence of monoterpene ozonolysis on NPF events, our data was limited and we acknowledge that other factors may have influenced nighttime NPF.

The COALA-2020 campaign highlights the significant role of biogenic emissions, particularly monoterpenes driving NPF and isoprene enhancing particle growth in Southeast Australia. These findings contribute to a better understanding of local atmospheric chemistry and its potential impact on regional air quality and climate. However, longer-term observations are necessary to capture the full picture of seasonal variations and non-fire related extreme events.

Supplementary Materials:

Author Contributions:

The experiment design was made by Clare Paton-Walsh (Murphy) and Melita Keywood.

The data collection was done by Jack Simmons, Travis Naylor, Paton-Walsh (Murphy), Asher Mouat, Melita Keywood, Ruhi Humpries, Malcolm Possell and Jhonathan Ramirez-Gamboa.

The data processing to convert mass spectra to concentration of VOCs was done by Asher Mouat under the direction and supervision of Jennifer Kaiser.

The data analysis was done by Jhonathan Ramirez-Gamboa

The paper was written by Jhonathan Ramirez-Gamboa and Clare Paton-Walsh (Murphy).

Funding:

COALA-2020 was supported by Australia's National Environmental Science Program through the Clean Air and Urban Landscapes hub. Jhonathan Ramirez-Gamboa was supported during his PhD studies by a commonwealth funded University Post-Graduate Award at the University of Wollongong.

Data Availability Statement:

Data is available at PANGEA via the following links:

- VOCs: https://doi.org/10.1594/PANGAEA.927277
- Aerosol size distributions: https://doi.org/10.1594/PANGAEA.928853
- Condensations nuclei > 3 nm in diameter: https://doi.org/10.1594/PANGAEA.925555
- Cloud condensation nuclei: https://doi.org/10.1594/PANGAEA.928925
- Green-house gases: https://doi.org/10.1594/PANGAEA.927313
- Air Quality data: https://doi.org/10.1594/PANGAEA.929001
- Meteorological data: https://doi.org/10.1594/PANGAEA.928929
- ACSM data: https://doi.org/10.1594/PANGAEA.973272

Acknowledgments:

We are grateful to all who contributed to the COALA-2020 campaign. Particular thanks are due to all the staff at Cataract Scout Camp and research students and staff: Ian Galbally, Kathryn Emmerson, Gunashanhar Gunaratnam, John Kirkwood, Warren White, David Griffiths, Alex Carter, Alan Griffiths, Hamish McDougall and Graham Kettlewell.

Conflicts of Interest:

The authors declare no conflicts of interest.

References

ABARES: Australian forest profiles 2019: Eucalypt, Australian Bureau of Agricultural Resource Economics and Sciences (ABARES), 2019.

Annesi-Maesano, I., Baiz, N., Banerjee, S., Rudnai, P., Rive, S., and the, S. G.: Indoor Air Quality and Sources in Schools and Related Health Effects, J. Toxicol. Environ. Health Part B, 16, 491–550, https://doi.org/10.1080/10937404.2013.853609, 2013.

Aydin, Y. M., Yaman, B., Koca, H., Dasdemir, O., Kara, M., Altiok, H., Dumanoglu, Y., Bayram, A., Tolunay, D., Odabasi, M., and Elbir, T.: Biogenic volatile organic compound (BVOC) emissions from forested areas in Turkey: Determination of specific emission rates for thirty-one tree species, Sci. Total Environ., 490, 239–253, https://doi.org/10.1016/J.SCITOTENV.2014.04.132, 2014.

Bianchi, F., Kurtén, T., Riva, M., Mohr, C., Rissanen, M. P., Roldin, P., Berndt, T., Crounse, J. D., Wennberg, P. O., Mentel, T. F., Wildt, J., Junninen, H., Jokinen, T., Kulmala, M., Worsnop, D. R., Thornton, J. A., Donahue, N., Kjaergaard, H. G., and Ehn, M.: Highly Oxygenated Organic Molecules (HOM) from Gas-Phase Autoxidation Involving Peroxy Radicals: A Key Contributor to Atmospheric Aerosol, Chem. Rev., 119, 3472–3509, https://doi.org/10.1021/acs.chemrev.8b00395, 2019.

Bousiotis, D., Brean, J., Pope, F. D., Dall'Osto, M., Querol, X., Alastuey, A., Perez, N., Petäjä, T., Massling, A., Nøjgaard, J. K., Nordstrøm, C., Kouvarakis, G., Vratolis, S., Eleftheriadis, K., Niemi, J. V., Portin, H., Wiedensohler, A., Weinhold, K., Merkel, M., Tuch, T., and Harrison, R. M.: The effect of meteorological conditions and atmospheric composition in the occurrence and

development of new particle formation (NPF) events in Europe, Atmospheric Chem. Phys., 21, 3345–3370, https://doi.org/10.5194/acp-21-3345-2021, 2021.

Chen, Z., Schofield, R., Rayner, P., Zhang, T., Liu, C., Vincent, C., Fiddes, S., Ryan, R. G., Alroe, J., Ristovski, Z. D., Humphries, R. S., Keywood, M. D., Ward, J., Paton-Walsh, C., Naylor, T., and Shu, X.: Characterization of aerosols over the Great Barrier Reef: The influence of transported continental sources, Sci. Total Environ., 690, 426–437, https://doi.org/10.1016/j.scitotenv.2019.07.007, 2019.

Dada, L., Ylivinkka, I., Baalbaki, R., Li, C., Guo, Y., Yan, C., Yao, L., Sarnela, N., Jokinen, T., Daellenbach, K. R., Yin, R., Deng, C., Chu, B., Nieminen, T., Wang, Y., Lin, Z., Thakur, R. C., Kontkanen, J., Stolzenburg, D., Sipilä, M., Hussein, T., Paasonen, P., Bianchi, F., Salma, I., Weidinger, T., Pikridas, M., Sciare, J., Jiang, J., Liu, Y., Petäjä, T., Kerminen, V.-M., and Kulmala, M.: Sources and sinks driving sulfuric acid concentrations in contrasting environments: implications on proxy calculations, Atmospheric Chem. Phys., 20, 11747–11766, https://doi.org/10.5194/acp-20-11747-2020, 2020.

Dada, L., Stolzenburg, D., Simon, M., Fischer, L., Heinritzi, M., Wang, M., Xiao, M., Vogel, A. L., Ahonen, L., Amorim, A., Baalbaki, R., Baccarini, A., Baltensperger, U., Bianchi, F., Daellenbach, K. R., DeVivo, J., Dias, A., Dommen, J., Duplissy, J., Finkenzeller, H., Hansel, A., He, X.-C., Hofbauer, V., Hoyle, C. R., Kangasluoma, J., Kim, C., Kürten, A., Kvashnin, A., Mauldin, R., Makhmutov, V., Marten, R., Mentler, B., Nie, W., Petäjä, T., Quéléver, L. L. J., Saathoff, H., Tauber, C., Tome, A., Molteni, U., Volkamer, R., Wagner, R., Wagner, A. C., Wimmer, D., Winkler, P. M., Yan, C., Zha, Q., Rissanen, M., Gordon, H., Curtius, J., Worsnop, D. R., Lehtipalo, K., Donahue, N. M., Kirkby, J., El Haddad, I., and Kulmala, M.: Role of sesquiterpenes in biogenic new particle formation, Sci. Adv., 9, eadi5297, https://doi.org/10.1126/sciadv.adi5297, 2023.

Dal Maso, M., Kulmala, M., Riipinen, I., and Wagner, R.: Formation and growth of fresh atmospheric aerosols: Eight years of aerosol size distribution data from SMEAR II, Hyytiälä, Finland, Boreal Environ. Res., 10, 323–336, 2005.

Du, W., Sun, Y. L., Xu, Y. S., Jiang, Q., Wang, Q. Q., Yang, W., Wang, F., Bai, Z. P., Zhao, X. D., and Yang, Y. C.: Chemical characterization of submicron aerosol and particle growth events at a national background site (3295 m a.s.l.) on the Tibetan Plateau, Atmospheric Chem. Phys., 15, 10811–10824, https://doi.org/10.5194/acp-15-10811-2015, 2015.

Emmerson, K., Possell, M., J. Aspinwall, M., Pfautsch, S., and G. Tjoelker, M.: Temperature response measurements from eucalypts give insight into the impact of Australian isoprene emissions on air quality in 2050, Atmospheric Chem. Phys., 20, 6193–6206, https://doi.org/10.5194/acp-20-6193-2020, 2020.

Emmerson, K. M., Galbally, I. E., Guenther, A. B., Paton-Walsh, C., Guerette, E.-A. A., Cope, M. E., Keywood, M. D., Lawson, S. J., Molloy, S. B., Dunne, E., Thatcher, M., Karl, T., and Maleknia, S. D.: Current estimates of biogenic emissions from eucalypts uncertain for southeast Australia, Atmospheric Chem. Phys., 16, 6997–7011, https://doi.org/10.5194/acp-16-6997-2016, 2016.

Emmerson, K. M., Cope, M. E., Galbally, I. E., Lee, S., and Nelson, P. F.: Isoprene and monoterpene emissions in south-east Australia: Comparison of a multi-layer canopy model with MEGAN and with atmospheric observations, Atmospheric Chem. Phys., 18, 7539–7556, https://doi.org/10.5194/acp-18-7539-2018, 2018.

Emmerson, K. M., Palmer, P. I., Thatcher, M., Haverd, V., and Guenther, A. B.: Sensitivity of isoprene emissions to drought over south-eastern Australia: Integrating models and satellite observations of soil moisture, Atmos. Environ., 209, 112–124, https://doi.org/10.1016/j.atmosenv.2019.04.038, 2019.

Fini, A., Brunetti, C., Loreto, F., Centritto, M., Ferrini, F., and Tattini, M.: Isoprene responses and functions in plants challenged by environmental pressures associated to climate change, Front. Plant Sci., 8, https://doi.org/10.3389/fpls.2017.01281, 2017.

Friedman, B. and Farmer, D.: SOA and gas phase organic acid yields from the sequential photooxidation of seven monoterpenes, Atmos. Environ., 187, https://doi.org/10.1016/j.atmosenv.2018.06.003, 2018.

Goldstein, A. H. and Galbally, I. E.: Known and unexplored organic constituents in the earth's atmosphere, Environ. Sci. Technol., 41, 1514–1521, https://doi.org/10.1021/es072476p, 2007.

Guenther, A., Jiang, X., Heald, C. L., Sakulyanontvittaya, T., Duhl, T., Emmons, L. K., and Wang, X.: The Model of Emissions of Gases and Aerosols from Nature version 2.1 (MEGAN2.1): an extended and updated framework for modeling biogenic emissions, Geosci. Model Dev., 5, 1471–1492, https://doi.org/10.5194/gmd-5-1471-2012, 2012.

Heinritzi, M., Dada, L., Simon, M., Stolzenburg, D., Wagner, A. C., Fischer, L., Ahonen, L. R., Amanatidis, S., Baalbaki, R., Baccarini, A., Bauer, P. S., Baumgartner, B., Bianchi, F., Brilke, S., Chen, D., Chiu, R., Dias, A., Dommen, J., Duplissy, J., Finkenzeller, H., Frege, C., Fuchs, C., Garmash, O., Gordon, H., Granzin, M., El Haddad, I., He, X., Helm, J., Hofbauer, V., Hoyle, C. R., Kangasluoma, J., Keber, T., Kim, C., Kürten, A., Lamkaddam, H., Laurila, T. M., Lampilahti, J., Lee, C. P., Lehtipalo, K., Leiminger, M., Mai, H., Makhmutov, V., Manninen, H. E., Marten, R., Mathot, S., Mauldin, R. L., Mentler, B., Molteni, U., Müller, T., Nie, W., Nieminen, T., Onnela, A., Partoll, E., Passananti, M., Petäjä, T., Pfeifer, J., Pospisilova, V., Quéléver, L. L. J., Rissanen, M. P., Rose, C., Schobesberger, S., Scholz, W., Scholze, K., Sipilä, M., Steiner, G., Stozhkov, Y., Tauber, C., Tham, Y. J., Vazquez-Pufleau, M., Virtanen, A., Vogel, A. L., Volkamer, R., Wagner, R., Wang, M., Weitz, L., Wimmer, D., Xiao, M., Yan, C., Ye, P., Zha, Q., Zhou, X., Amorim, A., Baltensperger, U., Hansel, A., Kulmala, M., Tomé, A., Winkler, P. M., Worsnop, D. R., Donahue, N. M., Kirkby, J., and Curtius, J.: Molecular understanding of the suppression of new-particle formation by isoprene, Atmospheric Chem. Phys., 20, 11809–11821, https://doi.org/10.5194/acp-20-11809-2020, 2020.

Higgins, D. N., Taylor, M. S. Jr., Krasnomowitz, J. M., and Johnston, M. V.: Growth Rate Dependence of Secondary Organic Aerosol on Seed Particle Size, Composition, and Phase, ACS Earth Space Chem., 6, 2158–2166, https://doi.org/10.1021/acsearthspacechem.2c00049, 2022.

Hu, W. W., Campuzano-Jost, P., Palm, B. B., Day, D. A., Ortega, A. M., Hayes, P. L., Krechmer, J. E., Chen, Q., Kuwata, M., Liu, Y. J., de Sá, S. S., McKinney, K., Martin, S. T., Hu, M., Budisulistiorini, S. H., Riva, M., Surratt, J. D., St. Clair, J. M., Isaacman-Van Wertz, G., Yee, L. D., Goldstein, A. H., Carbone, S., Brito, J., Artaxo, P., de Gouw, J. A., Koss, A., Wisthaler, A., Mikoviny, T., Karl, T., Kaser, L., Jud, W., Hansel, A., Docherty, K. S., Alexander, M. L., Robinson, N. H., Coe, H., Allan, J. D., Canagaratna, M. R., Paulot, F., and Jimenez, J. L.: Characterization of a real-time tracer for isoprene epoxydiols-derived secondary organic aerosol (IEPOX-SOA) from aerosol mass spectrometer measurements, Atmospheric Chem. Phys., 15, 11807–11833, https://doi.org/10.5194/acp-15-11807-2015, 2015.

Hussein, T., Dal Maso, M., Petäjä, T., Koponen, I., Paatero, P., Aalto, P., Hämeri, K., and Kulmala, M.: Evaluation of an automatic algorithm for fitting the particle number size distribution, Boreal Environ. Res., 10, 337–355, 2005.

Iyer, S., Rissanen, M. P., Valiev, R., Barua, S., Krechmer, J. E., Thornton, J., Ehn, M., and Kurtén, T.: Molecular mechanism for rapid autoxidation in α-pinene ozonolysis, Nat. Commun., 12, 878, https://doi.org/10.1038/s41467-021-21172-w, 2021.

Kalkavouras, P., Bougiatioti, A., Grivas, G., Stavroulas, I., Kalivitis, N., Liakakou, E., Gerasopoulos, E., Pilinis, C., and Mihalopoulos, N.: On the regional aspects of new particle formation in the Eastern Mediterranean: A comparative study between a background and an urban site based on long term observations, Atmospheric Res., 239, 104911, https://doi.org/10.1016/j.atmosres.2020.104911, 2020.

Kari, E., Hao, L., Ylisirniö, A., Buchholz, A., Leskinen, A., Yli-Pirilä, P., Nuutinen, I., Kuuspalo, K., Jokiniemi, J., Faiola, C. L., Schobesberger, S., and Virtanen, A.: Potential dual effect of anthropogenic emissions on the formation of biogenic secondary organic aerosol (BSOA), Atmospheric Chem. Phys., 19, 15651–15671, https://doi.org/10.5194/acp-19-15651-2019, 2019.

Kerminen, V.-M., Paramonov, M., Anttila, T., Riipinen, I., Fountoukis, C., Korhonen, H., Asmi, E., Laakso, L., Lihavainen, H., Swietlicki, E., Svenningsson, B., Asmi, A., Pandis, S. N., Kulmala, M., and Petäjä, T.: Cloud condensation nuclei production associated with atmospheric nucleation: a synthesis based on existing literature and new results, Atmospheric Chem. Phys., 12, 12037–12059, https://doi.org/10.5194/acp-12-12037-2012, 2012.

Kesselmeier, J. and Staudt, M.: Biogenic Volatile Organic Compounds (VOC): An Overview on Emission, Physiology and Ecology, J. Atmospheric Chem., 33, 23–88, https://doi.org/10.1023/A:1006127516791, 1999.

Keywood, M., Selleck, P., Galbally, I., Lawson, S., Powell, J., Cheng, M., Gillett, R., Ward, J., Harnwell, J., Dunne, E., Boast, K., Reisen, F., Molloy, S., Griffiths, A., Chambers, S., Humphries, R., Guerette, E.-A., Cohen, D. (2016):, Crumeyrolle, S., Zhang, C., Zeng, J., and Fedele, R.: Sydney Particle Study 2 - Aerosol and gas data collection. v1., edited by: CSIRO, , https://doi.org/10.4225/08/57903B83D6A5D, 2016.

Kiendler-Scharr, A., Wildt, J., Maso, M. D., Hohaus, T., Kleist, E., Mentel, T. F., Tillmann, R., Uerlings, R., Schurr, U., and Wahner, A.: New particle formation in forests inhibited by isoprene emissions, Nature, 461, 381–384, 2009.

Kirkby, J., Amorim, A., Baltensperger, U., Carslaw, K. S., Christoudias, T., Curtius, J., Donahue, N. M., Haddad, I. E., Flagan, R. C., Gordon, H., Hansel, A., Harder, H., Junninen, H., Kulmala, M., Kürten, A., Laaksonen, A., Lehtipalo, K., Lelieveld, J., Möhler, O., Riipinen, I., Stratmann, F., Tomé, A., Virtanen, A., Volkamer, R., Winkler, P. M., and Worsnop, D. R.: Atmospheric new particle formation from the CERN CLOUD experiment, Nat. Geosci., 16, 948–957, https://doi.org/10.1038/s41561-023-01305-0, 2023.

Kulmala, M., Maso, M. D., Mäkelä, J. M., Pirjola, L., Väkevä, M., Aalto, P., Miikkulainen, P., Hämeri, K., and O'dowd, C. D.: On the formation, growth and composition of nucleation mode particles, Tellus B, 53, 479–490, https://doi.org/10.1034/j.1600-0889.2001.530411.x, 2001.

Lee, B. H., Iyer, S., Kurtén, T., Varelas, J. G., Luo, J., Thomson, R. J., and Thornton, J. A.: Ring-opening yields and auto-oxidation rates of the resulting peroxy radicals from OH-oxidation of α-pinene and β-pinene, Environ. Sci. Atmospheres, 3, 399–407, https://doi.org/10.1039/D2EA00133K, 2023.

Lehtipalo, K., Yan, C., Dada, L., Bianchi, F., Xiao, M., Wagner, R., Stolzenburg, D., Ahonen, L. R., Amorim, A., Baccarini, A., Bauer, P. S., Baumgartner, B., Bergen, A., Bernhammer, A.-K., Breitenlechner, M., Brilke, S., Buchholz, A., Mazon, S. B., Chen, D., Chen, X., Dias, A., Dommen, J., Draper, D. C., Duplissy, J., Ehn, M., Finkenzeller, H., Fischer, L., Frege, C., Fuchs, C., Garmash, O., Gordon, H., Hakala, J., He, X., Heikkinen, L., Heinritzi, M., Helm, J. C., Hofbauer, V., Hoyle, C. R., Jokinen, T., Kangasluoma, J., Kerminen, V.-M., Kim, C., Kirkby, J., Kontkanen, J., Kürten, A., Lawler, M. J., Mai, H., Mathot, S., Mauldin, R. L., Molteni, U., Nichman, L., Nie, W., Nieminen, T., Ojdanic, A., Onnela, A., Passananti, M., Petäjä, T., Piel, F., Pospisilova, V.,

Quéléver, L. L. J., Rissanen, M. P., Rose, C., Sarnela, N., Schallhart, S., Schuchmann, S., Sengupta, K., Simon, M., Sipilä, M., Tauber, C., Tomé, A., Tröstl, J., Väisänen, O., Vogel, A. L., Volkamer, R., Wagner, A. C., Wang, M., Weitz, L., Wimmer, D., Ye, P., Ylisirniö, A., Zha, Q., Carslaw, K. S., Curtius, J., Donahue, N. M., Flagan, R. C., Hansel, A., Riipinen, I., Virtanen, A., Winkler, P. M., Baltensperger, U., Kulmala, M., and Worsnop, D. R.: Multicomponent new particle formation from sulfuric acid, ammonia, and biogenic vapors, Sci. Adv., 4, eaau5363, https://doi.org/10.1126/sciadv.aau5363, 2018.

Li, D., Huang, W., Wang, D., Wang, M., Thornton, J. A., Caudillo, L., Rörup, B., Marten, R., Scholz, W., Finkenzeller, H., Marie, G., Baltensperger, U., Bell, D. M., Brasseur, Z., Curtius, J., Dada, L., Duplissy, J., Gong, X., Hansel, A., He, X.-C., Hofbauer, V., Junninen, H., Krechmer, J. E., Kürten, A., Lamkaddam, H., Lehtipalo, K., Lopez, B., Ma, Y., Mahfouz, N. G. A., Manninen, H. E., Mentler, B., Perrier, S., Petäjä, T., Pfeifer, J., Philippov, M., Schervish, M., Schobesberger, S., Shen, J., Surdu, M., Tomaz, S., Volkamer, R., Wang, X., Weber, S. K., Welti, A., Worsnop, D. R., Wu, Y., Yan, C., Zauner-Wieczorek, M., Kulmala, M., Kirkby, J., Donahue, N. M., George, C., El-Haddad, I., Bianchi, F., and Riva, M.: Nitrate Radicals Suppress Biogenic New Particle Formation from Monoterpene Oxidation, Environ. Sci. Technol., 58, 1601–1614, https://doi.org/10.1021/acs.est.3c07958, 2024.

Liu, D., Zhang, Y., Zhong, S., Chen, S., Xie, Q., Zhang, D., Zhang, Q., Hu, W., Deng, J., Wu, L., Ma, C., Tong, H., and Fu, P.: Large differences of highly oxygenated organic molecules (HOMs) and low-volatile species in secondary organic aerosols (SOAs) formed from ozonolysis of β-pinene and limonene, Atmospheric Chem. Phys., 23, 8383–8402, https://doi.org/10.5194/acp-23-8383-2023, 2023.

Liu, J., D'Ambro, E. L., Lee, B. H., Lopez-Hilfiker, F. D., Zaveri, R. A., Rivera-Rios, J. C., Keutsch, F. N., Iyer, S., Kurten, T., Zhang, Z., Gold, A., Surratt, J. D., Shilling, J. E., and Thornton, J. A.: Efficient Isoprene Secondary Organic Aerosol Formation from a Non-IEPOX Pathway, Environ. Sci. Technol., 50, 9872–9880, https://doi.org/10.1021/acs.est.6b01872, 2016a.

Liu, X., Zhu, H., Hu, Y., Feng, S., Chu, Y., Wu, Y., Wang, C., Zhang, Y., Yuan, Z., and Lu, Y.: Public's Health Risk Awareness on Urban Air Pollution in Chinese Megacities: The Cases of Shanghai, Wuhan and Nanchang, Int. J. Environ. Res. Public. Health, 13, 845, 2016b.

Liu, Z., Chen, H., Li, L., Xie, G., Ouyang, H., Tang, X., Ju, R., Li, B., Zhang, R., and Chen, J.-M.: Real-time single particle characterization of oxidized organic aerosols in the East China Sea, Npj Clim. Atmospheric Sci., 5, 47, https://doi.org/10.1038/s41612-022-00267-1, 2022.

Luo, Y., Thomsen, D., Iversen, E. M., Roldin, P., Skønager, J. T., Li, L., Priestley, M., Pedersen, H. B., Hallquist, M., Bilde, M., Glasius, M., and Ehn, M.: Formation and temperature dependence of highly oxygenated organic molecules (HOMs) from Δ^3-carene ozonolysis, Atmospheric Chem. Phys., 24, 9459–9473, https://doi.org/10.5194/acp-24-9459-2024, 2024.

Mahilang, M., Deb, M. K., and Pervez, S.: Biogenic secondary organic aerosols: A review on formation mechanism, analytical challenges and environmental impacts, Chemosphere, 262, 127771, https://doi.org/10.1016/j.chemosphere.2020.127771, 2021.

Matsui, K.: Green leaf volatiles: hydroperoxide lyase pathway of oxylipin metabolism., Curr. Opin. Plant Biol., 9, 274–280, 2006.

Mouat, A. P., Paton-Walsh, C., Simmons, J. B., Ramirez-Gamboa, J., Griffith, D. W. T., and Kaiser, J.: Measurement report: Observations of long-lived volatile organic compounds from the 2019–2020 Australian wildfires during the COALA campaign, Atmospheric Chem. Phys., 22, 11033–11047, https://doi.org/10.5194/acp-22-11033-2022, 2022.

Nestorowicz, K., Jaoui, M., Rudzinski, K. J., Lewandowski, M., Kleindienst, T. E., Spólnik, G., Danikiewicz, W., and Szmigielski, R.: Chemical composition of isoprene SOA under acidic and non-acidic conditions: effect of relative humidity, Atmospheric Chem. Phys., 18, 18101–18121, https://doi.org/10.5194/acp-18-18101-2018, 2018.

Ormeño, E., Mévy, J. P., Vila, B., Bousquet-Mélou, A., Greff, S., Bonin, G., and Fernandez, C.: Water deficit stress induces different monoterpene and sesquiterpene emission changes in Mediterranean species. Relationship between terpene emissions and plant water potential, Chemosphere, 67, 276–284, https://doi.org/10.1016/J.CHEMOSPHERE.2006.10.029, 2007.

Ortega, I. K., Suni, T., Boy, M., Grönholm, T., Manninen, H. E., Nieminen, T., Ehn, M., Junninen, H., Hakola, H., Hellén, H., Valmari, T., Arvela, H., Zegelin, S., Hughes, D., Kitchen, M., Cleugh, H., Worsnop, D. R., Kulmala, M., and Kerminen, V.-M.: New insights into nocturnal nucleation, Atmospheric Chem. Phys., 12, 4297–4312, https://doi.org/10.5194/acp-12-4297-2012, 2012.

Padhy, P. K. K. and Varshney, C. K. K.: Emission of volatile organic compounds (VOC) from tropical plant species in India, Chemosphere, 59, 1643–1653, 2005.

Parworth, C., Fast, J., Mei, F., Shippert, T., Sivaraman, C., Tilp, A., Watson, T., and Zhang, Q.: Long-term measurements of submicrometer aerosol chemistry at the Southern Great Plains (SGP) using an Aerosol Chemical Speciation Monitor (ACSM), Atmos. Environ., 106, 43–55, https://doi.org/10.1016/j.atmosenv.2015.01.060, 2015.

Paton-Walsh, C., Rayner, P., Simmons, J., Fiddes, S. L., Schofield, R., Bridgman, H., Beaupark, S., Broome, R., Chambers, S. D., Chang, L. T.-C., Cope, M., Cowie, C. T., Desservettaz, M., Dominick, D., Emmerson, K., Forehead, H., Galbally, I. E., Griffiths, A., Guérette, É.-A., Haynes, A., Heyworth, J., Jalaludin, B., Kan, R., Keywood, M., Monk, K., Morgan, G. G., Nguyen Duc, H., Phillips, F., Popek, R., Scorgie, Y., Silver, J. D., Utembe, S., Wadlow, I., Wilson, S. R., and Zhang, Y.: A Clean Air Plan for Sydney: An Overview of the Special Issue on Air Quality in New South Wales, Atmosphere, 10, 774, 2019.

Paton-Walsh, C., Emmerson, K. M., Garland, R. M., Keywood, M., Hoelzemann, J. J., Huneeus, N., Buchholz, R. R., Humphries, R. S., Altieri, K., Schmale, J., Wilson, S. R., Labuschagne, C., Kalisa, E., Fisher, J. A., Deutscher, N. M., van Zyl, P. G., Beukes, J. P., Joubert, W., Martin, L., Mkololo, T., Barbosa, C., de Fatima Andrade, M., Schofield, R., Mallet, M. D., Harvey, M. J., Formenti, P., Piketh, S. J., and Olivares, G.: Key challenges for tropospheric chemistry in the Southern Hemisphere, Elem. Sci. Anthr., 10, 00050, https://doi.org/10.1525/elementa.2021.00050, 2022.

Peräkylä, O., Riva, M., Heikkinen, L., Quéléver, L., Roldin, P., and Ehn, M.: Experimental investigation into the volatilities of highly oxygenated organic molecules (HOMs), Atmospheric Chem. Phys., 20, 649–669, https://doi.org/10.5194/acp-20-649-2020, 2020.

Petit, J.-E., Favez, O., Sciare, J., Crenn, V., Sarda-Estève, R., Bonnaire, N., Močnik, G., Dupont, J.-C., Haeffelin, M., and Leoz-Garziandia, E.: Two years of near real-time chemical composition of submicron aerosols in the region of Paris using an Aerosol Chemical Speciation Monitor (ACSM) and a multi-wavelength Aethalometer, ATMOSPHERIC Chem. Phys., 15, 2985–3005, https://doi.org/10.5194/acp-15-2985-2015, 2015.

Phillips, F. A., Naylor, T., Forehead, H., Griffith, D. W. T., Kirkwood, J., and Paton-Walsh, C.: Vehicle Ammonia Emissions Measured in An Urban Environment in Sydney, Australia, Using Open Path Fourier Transform Infra-Red Spectroscopy, Atmosphere, 10, 208, 2019.

Pope, C. A. and Dockery, D. W.: Health effects of fine particulate air pollution: Lines that connect, J. Air Waste Manag. Assoc., 56, 709–742, 2006.

Pöschl, U.: Atmospheric Aerosols: Composition, Transformation, Climate and Health Effects, Angew. Chem. Int. Ed., 44, 7520–7540, https://doi.org/10.1002/anie.200501122, 2005.

Poulain, L., Spindler, G., Grüner, A., Tuch, T., Stieger, B., van Pinxteren, D., Petit, J.-E., Favez, O., Herrmann, H., and Wiedensohler, A.: Multi-year ACSM measurements at the central European research station Melpitz (Germany) – Part 1: Instrument robustness, quality assurance, and impact of upper size cutoff diameter, Atmospheric Meas. Tech., 13, 4973–4994, https://doi.org/10.5194/amt-13-4973-2020, 2020.

Ramirez-Gamboa, J., Paton-Walsh, C., Galbally, I., Simmons, J., Guerette, E.-A., Griffith, A. D., Chambers, S. D., and Williams, A. G.: Seasonal Variation of Biogenic and Anthropogenic VOCs in a Semi-Urban Area Near Sydney, Australia, Atmosphere, 12, 47, https://doi.org/10.3390/atmos12010047, 2021.

Ren, Y., Qu, Z., Du, Y., Xu, R., Ma, D., Yang, G., Shi, Y., Fan, X., Tani, A., Guo, P., Ge, Y., and Chang, J.: Air quality and health effects of biogenic volatile organic compounds emissions from urban green spaces and the mitigation strategies, Environ. Pollut., 230, 849–861, https://doi.org/10.1016/j.envpol.2017.06.049, 2017.

Riipinen, I., Yli-Juuti, T., Pierce, J. R., Petäjä, T., Worsnop, D. R., Kulmala, M., and Donahue, N. M.: The contribution of organics to atmospheric nanoparticle growth, Nat. Geosci., 5, 453–458, https://doi.org/10.1038/ngeo1499, 2012.

Riva, M., Heikkinen, L., Bell, D. M., Peräkylä, O., Zha, Q., Schallhart, S., Rissanen, M. P., Imre, D., Petäjä, T., Thornton, J. A., Zelenyuk, A., and Ehn, M.: Chemical transformations in monoterpene-derived organic aerosol enhanced by inorganic composition, Npj Clim. Atmospheric Sci., 2, 2, https://doi.org/10.1038/s41612-018-0058-0, 2019.

Schlag, P., Kiendler-Scharr, A., Blom, M. J., Canonaco, F., Henzing, J. S., Moerman, M., Prévôt, A. S. H., and Holzinger, R.: Aerosol source apportionment from 1-year measurements at the CESAR tower in Cabauw, the Netherlands, Atmospheric Chem. Phys., 16, 8831–8847, https://doi.org/10.5194/acp-16-8831-2016, 2016.

Shi, L. H., Zanobetti, A., Kloog, I., Coull, B. A., Koutrakis, P., Melly, S. J., and Schwartz, J. D.: Low-Concentration PM2.5 and Mortality: Estimating Acute and Chronic Effects in a Population-Based Study, Environ. Health Perspect., 124, 46–52, https://doi.org/10.1289/ehp.1409111, 2016.

Sihto, S.-L., Kulmala, M., Kerminen, V.-M., Dal Maso, M., Petäjä, T., Riipinen, I., Korhonen, H., Arnold, F., Janson, R., Boy, M., Laaksonen, A., and Lehtinen, K. E. J.: Atmospheric sulphuric acid and aerosol formation: implications from atmospheric measurements for nucleation and early growth mechanisms, Atmospheric Chem. Phys., 6, 4079–4091, https://doi.org/10.5194/acp-6-4079-2006, 2006.

Simmons, J. B., Paton-Walsh, C., Mouat, A. P., Kaiser, J., Humphries, R. S., Keywood, M., Griffith, D. W. T., Sutresna, A., Naylor, T., and Ramirez-Gamboa, J.: Bushfire smoke plume composition and toxicological assessment from the 2019–2020 Australian Black Summer, Air Qual. Atmosphere Health, 15, 2067–2089, https://doi.org/10.1007/s11869-022-01237-5, 2022.

Smit, R., Kingston, P., Neale, D. W., Brown, M. K., Verran, B., and Nolan, T.: Monitoring on-road air quality and measuring vehicle emissions with remote sensing in an urban area, Atmos. Environ., 218, 116978, https://doi.org/10.1016/j.atmosenv.2019.116978, 2019.

Song, M., Zhang, C., Wu, H., Mu, Y., Ma, Z., Zhang, Y., Liu, J., and Li, X.: The influence of OH concentration on SOA formation from isoprene photooxidation, Sci. Total Environ., 650, 951–957, https://doi.org/10.1016/j.scitotenv.2018.09.084, 2019.

Stangl, C. M., Krasnomowitz, J. M., Apsokardu, M. J., Tiszenkel, L., Ouyang, Q., Lee, S., and Johnston, M. V.: Sulfur Dioxide Modifies Aerosol Particle Formation and Growth by Ozonolysis of Monoterpenes and Isoprene, J. Geophys. Res. Atmospheres, 124, 4800–4811, https://doi.org/10.1029/2018JD030064, 2019.

Suni, T., Sogacheva, L., Lauros, J., Hakola, H., Bäck, J., Kurtén, T., Cleugh, H., van Gorsel, E., Briggs, P., Sevanto, S., and Kulmala, M.: Cold oceans enhance terrestrial new-particle formation in near-coastal forests, Atmospheric Chem. Phys., 9, 8639–8650, https://doi.org/10.5194/acp-9-8639-2009, 2009.

Takami, A., Miyoshi, T., Shimono, A., and Hatakeyama, S.: Chemical composition of fine aerosol measured by AMS at Fukue Island, Japan during APEX period, Atmos. Environ., 39, 4913–4924, https://doi.org/10.1016/j.atmosenv.2005.04.038, 2005.

Topping, D., Coe, H., McFiggans, G., Burgess, R., Allan, J., Alfarra, M. R., Bower, K., Choularton, T. W., Decesari, S., and Facchini, M. C.: Aerosol chemical characteristics from sampling conducted on the Island of Jeju, Korea during ACE Asia, Atmos. Environ., 38, 2111–2123, https://doi.org/10.1016/j.atmosenv.2004.01.022, 2004.

Tröstl, J., Chuang, W. K., Gordon, H., Heinritzi, M., Yan, C., Molteni, U., Ahlm, L., Frege, C., Bianchi, F., Wagner, R., Simon, M., Lehtipalo, K., Williamson, C., Craven, J. S., Duplissy, J., Adamov, A., Almeida, J., Bernhammer, A.-K., Breitenlechner, M., Brilke, S., Dias, A., Ehrhart, S., Flagan, R. C., Franchin, A., Fuchs, C., Guida, R., Gysel, M., Hansel, A., Hoyle, C. R., Jokinen, T., Junninen, H., Kangasluoma, J., Keskinen, H., Kim, J., Krapf, M., Kürten, A., Laaksonen, A., Lawler, M., Leiminger, M., Mathot, S., Möhler, O., Nieminen, T., Onnela, A., Petäjä, T., Piel, F. M., Miettinen, P., Rissanen, M. P., Rondo, L., Sarnela, N., Schobesberger, S., Sengupta, K., Sipilä, M., Smith, J. N., Steiner, G., Tomè, A., Virtanen, A., Wagner, A. C., Weingartner, E., Wimmer, D., Winkler, P. M., Ye, P., Carslaw, K. S., Curtius, J., Dommen, J., Kirkby, J., Kulmala, M., Riipinen, I., Worsnop, D. R., Donahue, N. M., and Baltensperger, U.: The role of low-volatility organic compounds in initial particle growth in the atmosphere, Nature, 533, 527–531, https://doi.org/10.1038/nature18271, 2016.

Uusitalo, H., Kontkanen, J., Ylivinkka, I., Ezhova, E., Demakova, A., Arshinov, M., Belan, B. D., Davydov, D., Ma, N., Petäjä, T., Wiedensohler, A., Kulmala, M., and Nieminen, T.: Occurrence of new particle formation events in Siberian and Finnish boreal forest, https://doi.org/10.5194/acp-2021-530, 2021.

Wang, S., Zhang, Q., Wang, G., Wei, Y., Wang, W., and Wang, Q.: The neglected autoxidation pathways for the formation of highly oxygenated organic molecules (HOMs) and the nucleation of the HOMs generated by limonene, Atmos. Environ., 304, 119727, https://doi.org/10.1016/j.atmosenv.2023.119727, 2023.

Wu, H., Li, Z., Li, H., Luo, K., Wang, Y., Yan, P., Hu, F., Zhang, F., Sun, Y., Shang, D., Liang, C., Zhang, D., Wei, J., Wu, T., Jin, X., Fan, X., Cribb, M., Fischer, M. L., Kulmala, M., and Petäjä, T.: The impact of the atmospheric turbulence-development tendency on new particle formation: a common finding on three continents, Natl. Sci. Rev., 8, nwaa157, https://doi.org/10.1093/nsr/nwaa157, 2021.

Zhang, H., Yee, L. D., Lee, B. H., Curtis, M. P., Worton, D. R., Isaacman-VanWertz, G., Offenberg, J. H., Lewandowski, M., Kleindienst, T. E., Beaver, M. R., Holder, A. L., Lonneman, W. A., Docherty, K. S., Jaoui, M., Pye, H. O. T., Hu, W., Day, D. A., Campuzano-Jost, P., Jimenez, J. L., Guo, H., Weber, R. J., de Gouw, J., Koss, A. R., Edgerton, E. S., Brune, W., Mohr, C., Lopez-Hilfiker, F. D., Lutz, A., Kreisberg, N. M., Spielman, S. R., Hering, S. V., Wilson, K. R., Thornton, J. A., and Goldstein, A. H.: Monoterpenes are the largest source of summertime organic aerosol in the southeastern United States, Proc. Natl. Acad. Sci., 115, 2038–2043, https://doi.org/10.1073/pnas.1717513115, 2018.

Zhang, J., Zhao, J., Luo, Y., Mickwitz, V., Worsnop, D., and Ehn, M.: On the potential use of highly oxygenated organic molecules (HOMs) as indicators for ozone formation sensitivity, Atmospheric Chem. Phys., 24, 2885–2911, https://doi.org/10.5194/acp-24-2885-2024, 2024.

Zhao, J., Smith, J. N., Eisele, F. L., Chen, M., Kuang, C., and McMurry, P. H.: Observation of neutral sulfuric acid-amine containing clusters in laboratory and ambient measurements, Atmospheric Chem. Phys., 11, 10823–10836, https://doi.org/10.5194/acp-11-10823-2011, 2011.

Zheng, J., Ma, Y., Chen, M., Zhang, Q., Wang, L., Khalizov, A. F., Yao, L., Wang, Z., Wang, X., and Chen, L.: Measurement of atmospheric amines and ammonia using the high resolution time-of-flight chemical ionization mass spectrometry, Atmos. Environ., 102, 249–259, https://doi.org/10.1016/j.atmosenv.2014.12.002, 2015.